Mon. Not. R. Astron. Soc. **000**, 1–26 (0000) Printed 11 December 2014 (MN LATEX style file v2.2)

The environmental dependence of the structure of galactic discs in STAGES S0 galaxies: implications for S0 formation

David T. Maltby,[1⋆] Alfonso Aragón-Salamanca,[1] Meghan E. Gray,[1] Carlos Hoyos,[2] Christian Wolf,[3] Shardha Jogee[4] and Asmus Böhm[5]
[1] *School of Physics and Astronomy, The University of Nottingham, University Park, Nottingham NG7 2RD*
[2] *Instituto de Astronomia, Geofísica e Ciências Atmosféricas, Rua do Matão 1226, Cidade Universitária São Paulo-SP, Brazil*
[3] *Research School of Astronomy and Astrophysics, Australian National University, Canberra, ACT 2611, Australia*
[4] *Department of Astronomy, University of Texas at Austin, 1 University Station, C1400 Austin, TX 78712-0259, USA*
[5] *Institute for Astro- and Particle Physics, University of Innsbruck, Technikerstr. 25/8, 6020 Innsbruck, Austria*

arXiv:1412.3167v1 [astro-ph.GA] 10 Dec 2014

Accepted Year Month Date. Received Year Month Date; in original form Year Month Date

ABSTRACT

We present an analysis of V-band radial surface brightness $\mu(r)$ profiles for S0 galaxies in different environments using *Hubble Space Telescope*/Advanced Camera for Surveys imaging and data from the Space Telescope A901/2 Galaxy Evolution Survey (STAGES). Using a large sample of ~ 280 field and cluster S0s, we find that in both environments, ~ 25 per cent have a pure exponential disc (Type I) and ~ 50 per cent exhibit an up-bending disc break (*antitruncation*, Type III). However, we find hardly any (< 5 per cent) down-bending disc breaks (*truncations*, Type II) in our S0s and many cases (~ 20 per cent) where no discernible exponential component was observed (i.e. general curvature). We also find no evidence for an environmental dependence on the disc scalelength h or break strength T (outer-to-inner scalelength ratio), implying that the galaxy environment does not affect the stellar distribution in S0 stellar discs. Comparing disc structure (e.g. h, T) between these S0s and the spiral galaxies from our previous studies, we find: i) no evidence for the Type I scalelength h being dependent on morphology; and ii) some evidence to suggest that the Type II/III break strength T is smaller (weaker) in S0s compared to spiral galaxies. Taken together, these results suggest that the stellar distribution in S0s is not drastically affected by the galaxy environment. However, some process inherent to the morphological transformation of spiral galaxies into S0s does affect stellar disc structure causing a weakening of $\mu(r)$ breaks and may even eliminate truncations from S0 galaxies. In further tests, we perform analytical bulge–disc decompositions on our S0s and compare the results to those for spiral galaxies from our previous studies. For Type III galaxies, we find that bulge light can account for the excess light at large radii in up to ~ 50 per cent of S0s but in only ~ 15 per cent of spirals. We propose that this result is consistent with a fading stellar disc (evolving bulge-to-disc ratio) being an inherent process in the transformation of spiral galaxies into S0s.

Key words: galaxies: clusters: individual: A901/2 — galaxies: elliptical and lenticular, cD — galaxies: evolution — galaxies: spiral — galaxies: structure.

1 INTRODUCTION

It is now well established that correlations exist between the properties of galaxies, e.g. morphology, colour and star-formation rate, and their local environment (Dressler 1980; Weinmann et al. 2006). However, the exact mechanisms driving these correlations remain elusive. Certain physical processes inherent to galaxy evolution and related to the galaxy environment may contribute, e.g. ram-pressure stripping of the interstellar medium, mergers and harassment (e.g. Gunn & Gott 1972; Icke 1985; Moore et al. 1996). However, the relative importance of each of these processes in galaxy evolution remains uncertain.

An important aspect in studying how the environment could affect the formation and evolution of disc galaxies is the structure of galactic discs. Their fragile outer regions are more easily affected by interactions with other galaxies, and therefore their structural characteristics must be closely related to their evolutionary history. Consequently, exploring

⋆ E-mail: dtmaltby@gmail.com

© 0000 RAS

the effect of the environment on the light distribution (surface brightness μ profile) of disc galaxies should aid in our understanding of the physical processes of galaxy evolution occurring in different environments.

The light profiles of disc galaxies are comprised of two main structural components: an inner bulge-dominated component; and an outer exponentially declining disc with some minor deviations related to substructure (de Vaucouleurs 1959; Freeman 1970). However, this 'classical' picture fails for the majority of disc galaxies in the Universe since the exponential component is often truncated (sharply cut off) after several scalelengths (van der Kruit 1979). In fact, most disc μ profiles are actually best described by a two slope model (broken exponential), characterised by an inner and outer exponential scalelength separated by a relatively well-defined break radius $r_{\rm brk}$ (Pohlen et al. 2002). Many studies have reported (mainly using surface photometry) the existence of broken exponential discs in both the local (Pohlen et al. 2002, 2007; Pohlen & Trujillo 2006; Bakos et al. 2008; Erwin et al. 2008, 2012; Gutiérrez et al. 2011; Maltby et al. 2012a) and distant $z < 1$ Universe (Pérez 2004; Trujillo & Pohlen 2005; Azzollini et al. 2008). Broken exponential discs have also been reported through the use of resolved star counts on some nearby galaxies (Ibata et al. 2005; Ferguson et al. 2007).

As a direct result of these studies, a comprehensive classification scheme for disc galaxies has emerged based on break features in the outer disc component of their radial $\mu(r)$ profiles (see e.g. Pohlen & Trujillo 2006; Erwin et al. 2008). This classification scheme consists of three broad types (Type I, II and III): Type I (no break) – the galaxy has a simple exponential profile extending out to several scalelengths (e.g. Bland-Hawthorn et al. 2005); Type II (down-bending break, *truncation*) – a broken exponential with a shallow inner and steeper outer region separated by a relatively well-defined break radius $r_{\rm brk}$ (van der Kruit 1979; Pohlen et al. 2002); Type III (up-bending break, *antitruncation*) – a broken exponential with the opposite behaviour to a Type II profile (a shallower region beyond $r_{\rm brk}$; Erwin et al. 2005). In each case the classification refers to the outer disc component of the galaxy $\mu(r)$ profile and does not consider the inner bulge component even if the bulge is near exponential in nature.

At present, the physical origins of the different profile types are not well understood. Some models suggest that Type II profiles (truncations) could be the consequence of a radial star formation threshold (e.g. Kennicutt 1989; Elmegreen & Parravano 1994; Schaye 2004). Others suggest that Type II profiles are caused by a resonance phenomenon and a redistribution of angular momentum (Debattista et al. 2006). However, most current theories incorporate both these ideas, suggesting that the inner disc forms as a consequence of a star formation threshold while the outer disc forms by the outward migration of stars from the inner disc to regions beyond the star formation threshold (i.e. break radius $r_{\rm brk}$). This proposed migration could be due to resonant scattering with spiral arms (Roškar et al. 2008a,b) or clump disruptions (Bournaud et al. 2007). For Type III profiles, their discovery is still very recent (Erwin et al. 2005) and therefore much less effort has been afforded to their origin. Erwin et al. (2005) suggest that in some cases the excess light beyond the break radius $r_{\rm brk}$ could actually be attributed to light from the spheroidal bulge or halo extending beyond the end of the disc; however, these cases seem to be quite rare (Maltby et al. 2012b). In general, it appears that Type III profiles are the consequence of a disturbed system and that recent minor mergers could produce up-bending stellar profiles in the remnant galaxy (Younger et al. 2007; Sil'Chenko et al. 2011).

Investigating the frequency of profile types for different morphologies and in regions of different galaxy density, is a useful tool for exploring galaxy evolution and the role of the galaxy environment. However, presently there have only been a few systematic searches for broken exponentials in stellar discs (e.g. Pohlen & Trujillo 2006; Azzollini et al. 2008; Erwin et al. 2008, 2012; Gutiérrez et al. 2011; Maltby et al. 2012a) and these rarely span the full range of disc morphologies (S0–Sdm). Pohlen & Trujillo (2006) use a local sample of ~ 90 late-type spirals (Sb–Sdm) and find that the distribution of profile types I:II:III is approximately 10:60:30 per cent. However, Erwin et al. (2008) use a local sample of 66 barred early-type disc galaxies (S0–Sb) and find a distribution of approximately 30:40:25 per cent (the remaining ~ 5 per cent contained both Type II and Type III features). The differences in the profile-type fractions between these two authors can easily be attributed to the morphological range of their respective samples. This is because the shape of disc galaxy $\mu(r)$ profiles is dependent on morphology (Pohlen & Trujillo 2006; Gutiérrez et al. 2011; Maltby et al. 2012a). Gutiérrez et al. (2011) explored this issue by combining their local sample of 47 unbarred early-type galaxies with those of Pohlen & Trujillo (2006) and Erwin et al. (2008) and examined the profile-type distribution across the entire S0–Sdm range. They find that towards later Hubble types (S0 $\rightarrow$ Sdm) the fraction of Type I profiles decreases ($\sim 30 \rightarrow 10$ per cent) and the fraction of Type II profiles increases ($\sim 25 \rightarrow 80$ per cent). Consequently, morphology is an important factor when comparing the profile-type distributions from these different studies.

Presently, the effect of the galaxy environment on the frequency of profile types has only been explored by a few authors. For spiral galaxies, Maltby et al. (2012a) use a sample of ~ 300 field and cluster spirals (Sa–Sdm) and find no environmental dependence on the distribution of profile types in the outer regions of the stellar disc ($\mu > 24\,{\rm mag\,arcsec^{-2}}$). We note that due to the limited surface brightness range studied by Maltby et al. (2012a), their profile type distributions cannot be directly compared to those of previous works. However, an inspection of their $\mu(r)$ profiles yields a profile type distribution I:II:III of approximately 10:50:40 per cent in both the field and cluster environment, which is in line with previous works. In contrast, for S0 galaxies Erwin et al. (2012) recently discovered an intriguing environmental dependence among the shapes of their $\mu(r)$ profiles. Using a sample of ~ 70 field and cluster S0s they find that in the field the distribution is 25:25:50 per cent while in the cluster the distribution is 50:0:50 per cent. Thus their cluster S0s show a complete lack of Type II profiles.

In this work, we expand on these environmental studies by performing a systematic search for broken exponential discs in field and cluster S0s using the Space Telescope A901/2 Galaxy Evolution Survey (STAGES; Gray et al.

2009). This work builds on previous studies by using larger and more statistically viable field and cluster samples and by being one of only a few studies to probe the high-density environments (see Erwin et al. 2012, for another example). This work is also similar to our companion study (Maltby et al. 2012a), which explores the effect of the galaxy environment on the disc structure of spiral galaxies in STAGES[1]. Since S0s are expected to have evolved from spiral galaxies, by comparing the results of these two works we aim to provide some insight into the potential evolutionary mechanisms involved in their morphological transformation.

The structure of this paper is as follows. In Section 2, we give a brief description of the STAGES data set relevant to this work and outline our sample selection in Section 2.1. In Section 3, we describe the method used to obtain our radial surface brightness $\mu(r)$ profiles from the STAGES V-band imaging and explain our profile classification scheme in Section 4. We present our results for S0 galaxies in Section 5, and then compare these results with those for STAGES spiral galaxies from Maltby et al. (2012a) in Section 6. In Section 7, we complement this work with an examination of the impact of a de Vaucouleurs (1948) bulge profile on the outer regions of our S0 $\mu(r)$ profiles, and compare our results with those from a similar study using spiral galaxies (Maltby et al. 2012b). Finally, we draw our conclusions in Section 8. Throughout this paper, we adopt a cosmology of $H_0 = 70\,\mathrm{km\,s^{-1}\,Mpc^{-1}}$, $\Omega_\Lambda = 0.7$ and $\Omega_\mathrm{m} = 0.3$, and use AB magnitudes unless stated otherwise.

2 DESCRIPTION OF THE DATA

This work is entirely based on the STAGES data published by Gray et al. (2009). STAGES is an extensive multiwavelength survey targeting the Abell(A) 901/902 multicluster system ($z \sim 0.167$) and covering a wide range of galaxy environments. These environments span from the general field to the intermediate densities of the A901/2 clusters (Heiderman et al. 2009). *Hubble Space Telescope* (*HST*)/Advanced Camera for Surveys (ACS) V-band (F606W) imaging covering the full $0.5^\circ \times 0.5^\circ$ ($\sim 5 \times 5\,\mathrm{Mpc}^2$) of the multicluster system is available and complemented by extensive multiwavelength observations. These include high-precision photometric redshifts and observed-/rest-frame spectral energy distributions (SEDs) from the 17-band COMBO-17 photometric redshift survey (Wolf et al. 2003). These photometric redshifts are accurate to 1 per cent in $\delta z/(1+z)$ at $R < 21$. However, photo-z quality degrades for progressively fainter galaxies reaching accuracies of 2 per cent for galaxies with $R \sim 22$ and 10 per cent for galaxies with $R > 24$ (Wolf et al. 2004, 2008). Stellar mass estimates derived from the SED fitting of the COMBO-17 photometry are also available (Borch et al. 2006; Gray et al. 2009).

Gray et al. (2009) have also performed Sérsic profile fitting using the GALFIT code (Peng et al. 2002) on all *HST*/ACS images and conducted simulations to quantify the completeness of the survey, all of which are publicly available[2]. Additionally, all galaxies with $R < 23.5$ and $z_\mathrm{phot} < 0.4$ (5090 galaxies) were visually classified by seven members of the STAGES team into Hubble-type morphologies (E, S0, Sa, Sb, Sc, Sd, Irr) and their intermediate classes (Gray et al., in preparation). This classification ignored bars and degrees of asymmetry and defined S0s to be disc galaxies with a visible bulge but no spiral arms (smooth disc).

2.1 Sample selection

Our sample of field and cluster S0 galaxies is drawn from Maltby et al. (2010). This consists of a large, mass-limited ($M_* > 10^9\,\mathrm{M}_\odot$), visually classified sample of 276 S0s from both the field and cluster environments in STAGES (60 field and 216 cluster). In the following, we give a brief summary of the relevant field and cluster sample selection presented in Maltby et al. (2010).

The cluster S0 sample is selected from a parent sample of cluster galaxies suggested for STAGES by Gray et al. (2009). This parent sample of cluster galaxies is defined solely from photometric redshifts. The photo-z distribution of cluster galaxies is assumed to be Gaussian while the distribution of field galaxies is assumed to be consistent with the average galaxy counts $N(z, R)$ outside the cluster and to vary smoothly with redshift and magnitude. Cluster galaxies are then defined simply via a redshift interval around the known spectroscopic redshift of the cluster, $z_\mathrm{phot} = [0.17 - \Delta z, 0.17 + \Delta z]$, the width of which varies with R-magnitude. The half-width Δz as a function of R-magnitude is

$$\Delta z(R) = \sqrt{0.015^2 + 0.0096525^2(1 + 10^{0.6[R_\mathrm{tot} - 20.5]})}. \quad (1)$$

This cluster selection adopts a narrow redshift range for bright R-magnitudes due to the high precision of the COMBO-17 photometric redshifts; however, the interval increases in width towards fainter R-magnitudes to accommodate for the increase in the photo-z error. Gray et al. (2009) calculate the completeness and contamination of this cluster selection as a function of R-magnitude by using the counts of their smooth models. In these calculations, they compromise Δz so that the completeness of the cluster selection is > 90 per cent at all magnitudes. The completeness of this selection converges to nearly 100 per cent for bright galaxies (see Gray et al. 2009, for further details). This cluster sample is then limited by stellar mass ($\log M_*/\mathrm{M}_\odot > 9$) and morphology (visually classified S0s) in order to create our final sample of 216 cluster S0 galaxies.

The field sample is selected from STAGES galaxies by applying a redshift interval either side of the cluster redshift ($z_\mathrm{cl} = 0.167$) that avoids the cluster selection. We use a lower redshift interval at $z = [0.05, 0.14]$ and an upper redshift interval at $z = [0.22, 0.30]$, based on a similar sample selection used by Wolf et al. (2009). This field sample is then limited by stellar mass ($\log M_*/\mathrm{M}_\odot > 9$) and morphology (visually classified S0s) in order to create our final sample of 60 field S0 galaxies. For full details of the field and cluster sample selection used in this work, see Maltby et al. (2010).

In the data catalogue published by Gray et al. (2009), there are two sets of derived values for galaxy properties such as magnitude and stellar mass: one value based on the photo-z estimate and another assuming the galaxy is located at the known spectroscopic redshift of the cluster ($z_\mathrm{cl} = 0.167$). In this work, we use the original photo-z es-

[1] Note: unlike Maltby et al. (2012a), in this work our break classification is based on the entire disc and *not* just the outer disc ($\mu > 24\,\mathrm{mag\,arcsec^{-2}}$) (see Section 4).
[2] http://www.nottingham.ac.uk/astronomy/stages

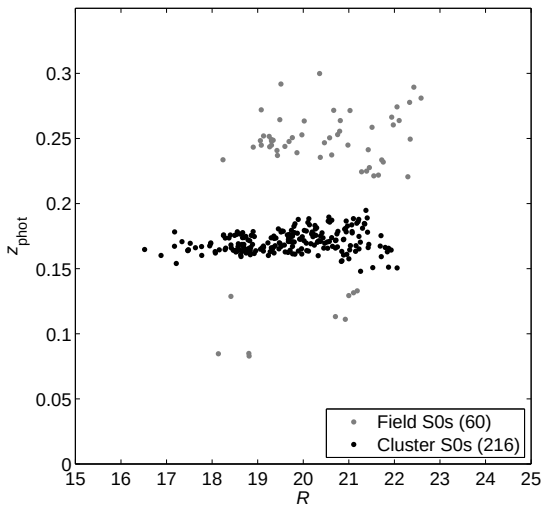

Figure 1. The photometric redshift $z_{\rm phot}$ versus total R-band magnitude (Vega) for the field (grey points) and cluster (black points) S0 galaxy samples. The field sample reaches $R \sim 23$ and the cluster sample reaches $R \sim 22$. Respective sample sizes are shown in the legend.

Table 1. Properties of the field and cluster S0 samples.

Property	Field	Cluster
$N_{\rm gal}$	60	216
Completeness	>70 per cent	>90 per cent
Contamination	–	<25 per cent
$R_{\rm mean}$	20.44	19.71
$M_{B(\rm min)}$	-16.54	-16.45
$M_{B(\rm max)}$	-21.19	-21.78
$z_{\rm phot,mean}$	0.230	0.171
$z_{\rm phot,min}$	0.083	0.148
$z_{\rm phot,max}$	0.300	0.195
$\log M_{*,\rm mean}$	10.41	10.45
Bar fraction	7 per cent	14 per cent

timates for our field sample and the fixed redshift values for our cluster sample. This practice prevents the propagation of photo-z errors into the physical values of our cluster galaxies.

The completeness of STAGES is $>$ 90 per cent for $R < 23.5$ (Gray et al. 2009) which is true for both our field and cluster S0 samples (see Fig. 1). However, based on previous COMBO-17 experience Wolf et al. (2009) estimate that at low stellar masses $M_* < 10^{9.5}\,{\rm M}_\odot$, the field sample could have an additional 20 per cent incompleteness. Consequently, our field sample is essentially $>$ 70 per cent complete. For our cluster sample, completeness is $>$ 90 per cent and contamination by the field is $<$ 25 per cent based on the R-magnitude the cluster sample reaches (see Fig. 1 and Gray et al. 2009: fig. 14)[3]. No further incompleteness is introduced by selecting only visually classified S0 galaxies (Maltby et al. 2010). The properties of the field and cluster S0 samples are shown in Table 1.

[3] Note: using spectroscopy, Bösch et al. (2013a) report that the contamination of this cluster sample may actually be $<$ 10 per cent.

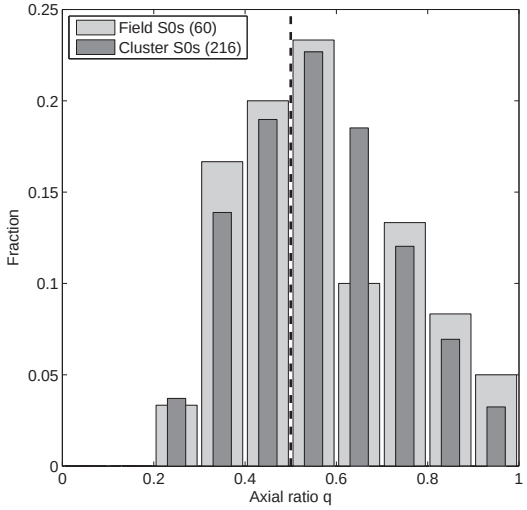

Figure 2. The distribution of minor-to-major axial ratio q for our field (light grey) and cluster (dark grey) S0 galaxies. The q cut used by previous works ($q > 0.5$, represented by a black dashed line) is shown for reference. Errors in q are $<$ 3 per cent. Respective sample sizes are shown in the legend.

2.2 Galaxy inclination

In the majority of studies that use surface photometry to explore broken exponential stellar discs, the disc galaxy samples are limited by galaxy inclination i to be face-on to intermediately inclined (e.g. Pohlen & Trujillo 2006; Erwin et al. 2008; Gutiérrez et al. 2011; Maltby et al. 2012a). In general, the minor-to-major axial ratio q ($q = b/a = 1 - e$, where a and b are the semimajor and semiminor axes, respectively, and e is the ellipticity) is restricted to correspond to an inclination i of less than 60° ($q > 0.5$ or $e < 0.5$). The purpose of this inclination i cut is to

(i) minimise the influence of dust on the galaxy $\mu(r)$ profiles – this is particularly important in the case of spiral galaxies, but less of an issue with S0s;
(ii) allow for reliable information on disc sub-structure, e.g. bars, rings and spiral arms;
(iii) ensure observations/measurements of the disc component can actually probe the disc light outside of the bulge-dominated region.

The axial ratio q for our S0 galaxies is determined from the STAGES GALFIT models (Gray et al. 2009) and the axial ratio q distributions for our field/cluster S0s are shown in Fig. 2. The suggested inclination cut ($q > 0.5$) would remove $\sim$ 40 per cent of our field and cluster S0s. Unfortunately, this would have a drastic effect on the number of galaxies in our field S0 sample and the quality of our field property distributions and subsequent results. Therefore, in order to maintain our field sample size, we do not limit our S0 samples by galaxy inclination i in this study. However, we take account of the above considerations by performing parallel analysis on both the full S0 sample and a low-axis ratio ($q > 0.5$) S0 sub-sample (36 field and 137 cluster S0s). Reassuringly, we find that the application of such an inclination i cut ($i < 60°$, $q > 0.5$) has no effect on the overall significance of our results or our conclusions.

3 PROFILE FITTING

For each galaxy in our field and cluster sample, we use the IRAF task ellipse[4] in order to obtain azimuthally-averaged radial surface brightness $\mu(r)$ profiles from the STAGES *HST*/ACS V-band imaging. The ACS images used include the sky background and the necessary sky subtraction is performed after profile fitting (see Section 3.1).

We run ellipse using bad pixel masks that remove all sources of contamination from our isophotal fits, e.g. background/companion galaxies and foreground stars (everything not associated with the galaxy itself). In this work, we use the bad pixel masks of Gray et al. (2009) but also apply some additional manual masking. Gray et al. (2009) use the data pipeline 'Galaxy Analysis over Large Areas: Parameter Assessment by GALFITting Objects from SExtractor' (GALAPAGOS; Barden et al. 2012) to extract source galaxies from the STAGES *HST*/ACS V-band imaging and fit Sérsic (1968) $\mu(r)$ models to each galaxy image using the GALFIT code (Peng et al. 2002). Bad pixel masks are automatically generated by GALAPAGOS for each galaxy image and in most cases the companion galaxies are completely masked out. However, occasionally in crowded regions GALFIT performs multiobject fitting and therefore the companion galaxies in these cases are not removed by the bad pixel masks as they are too close to the subject galaxy. In these cases (three field and 27 cluster, ~ 10 per cent), we remove the companion galaxies from the ACS image by the subtraction of their GALFIT surface brightness model. The residuals of these companion galaxies are not expected to have any significant effect on the azimuthally-averaged radial μ profile for the subject galaxy. However, we still modify the bad pixel masks of Gray et al. (2009) by applying some additional manual masking in order to remove these residual features and also some low surface brightness objects not detected by the GALAPAGOS pipeline.

Using a similar procedure to previous works (Pohlen & Trujillo 2006; Erwin et al. 2008; Maltby et al. 2012a), we fit two different sets of ellipses to each galaxy image[5]. The first is a free-parameter fit (fixed centre, free ellipticity e and position angle PA) and tends to follow morphological features such as bars and rings. Consequently, these free fits are not suitable for the characterisation of the underlying stellar disc studied in this paper. However, their $e(r)$ and PA(r) radial profiles may be used to determine the e and PA of the outer stellar disc component. This was achieved using an estimate for the semimajor axis of the end of the stellar disc $a_{\rm disc\,lim}$ (where the galaxy surface brightness enters the background noise) obtained from a visual inspection of the ACS image. A fixed-parameter fit (fixed centre, e and PA using the e and PA determined for the outer disc) is then used to produce our final measured $\mu(r)$ profiles. During these fixed-parameter fits, four iterations of a 3σ rejection are applied to deviant points below and above the average in order to smooth some of the bumps in the surface brightness profiles that are due to non-axisymmetric features, i.e. not part of the disc (e.g. star-forming regions and supernovae). The necessary sky subtraction is then performed using the sky level estimates of Gray et al. (2009) generated by the GALAPAGOS pipeline (see Section 3.1).

All our S0 $\mu(r)$ profiles are then corrected for Galactic foreground extinction, individual galaxy inclination i and surface brightness dimming (the μ profiles of our field galaxies, $0.05 < z_{\rm phot} < 0.30$, are corrected to the redshift of the cluster $z_{\rm cl} = 0.167$). Full details of the fitting procedure (performed on a different sample of galaxies), subsequent photometric calibration and an estimation of the error in the sky subtraction can be found in Maltby et al. (2012a).

3.1 Sky subtraction

During the GALFIT Sérsic model fitting performed by the GALAPAGOS pipeline (Gray et al. 2009), the sky level is calculated individually for each source galaxy by evaluating a flux growth curve and using the full science frame. In this paper, for each sample galaxy we use the sky level determined by GALAPAGOS ($sky_{\rm gal}$) for our sky subtraction. The 1σ error in this sky subtraction is ± 0.18 counts (see Maltby et al. 2012a).

For our $\mu(r)$ profiles, the error in the sky subtraction dominates over the individual errors produced by ellipse in the fitting process. At $\mu < 25\,{\rm mag\,arcsec^{-2}}$, the fit error dominates over the error in the sky subtraction but has a negligible effect on the $\mu(r)$ profile. However, at $\mu > 25\,{\rm mag\,arcsec^{-2}}$ the sky subtraction error dominates the error in the $\mu(r)$ profile. The sky subtraction error can have a significant effect on the $\mu(r)$ profile of the S0 galaxies, especially in the outer regions where the surface brightness μ approaches that of the sky background. However, for any particular galaxy the global sky subtraction error is approximately constant across the length of the $\mu(r)$ profile. Therefore, we can specify the error in our $\mu(r)$ profiles by generating profiles for when the sky background is oversubtracted and undersubtracted by $\pm 1\sigma$.

The $\pm 1\sigma$ error in the sky background corresponds to a critical surface brightness limit $\mu_{\rm crit}$ below which the sky subtracted $\mu(r)$ profile of a galaxy becomes unreliable. This critical surface brightness $\mu_{\rm crit}$ is approximately $27.7\,{\rm mag\,arcsec^{-2}}$. We also define a limiting surface brightness $\mu_{\rm lim}$, corresponding to a $\pm 3\sigma$ sky error, below which identifying profile breaks becomes unreliable. The limiting surface brightness $\mu_{\rm lim}$ is approximately $26.5\,{\rm mag\,arcsec^{-2}}$.

3.2 Reliability of the GALAPAGOS sky background

An initial inspection of our S0 $\mu(r)$ profiles revealed two key observations: i) many cases exhibiting significant curvature throughout the $\mu(r)$ profile; and ii) a distinct lack of truncations (Type II features). We wanted to ensure that these observations were not just the manifestation of a sky subtraction problem, causing the sky to be either oversubtracted or undersubtracted in our $\mu(r)$ profiles. Therefore, we assess the reliability of our sky subtraction by the comparison of our GALAPAGOS sky values $sky_{\rm gal}$ with an additional rough estimate for the sky background $sky_{\rm est}$.

For each S0 galaxy, we obtain this sky estimate $sky_{\rm est}$ by using pixels obtained from the four corners of the galaxy ACS image (postage stamp). The sizes of these ACS postage

[4] STSDAS package - version 2.12.2

[5] Note: all our isophotal fits use logarithmic radial sampling (steps – 0.03 dex) and a fixed isophotal centre (galaxy centre) determined from the GALFIT Sérsic model (Gray et al. 2009).

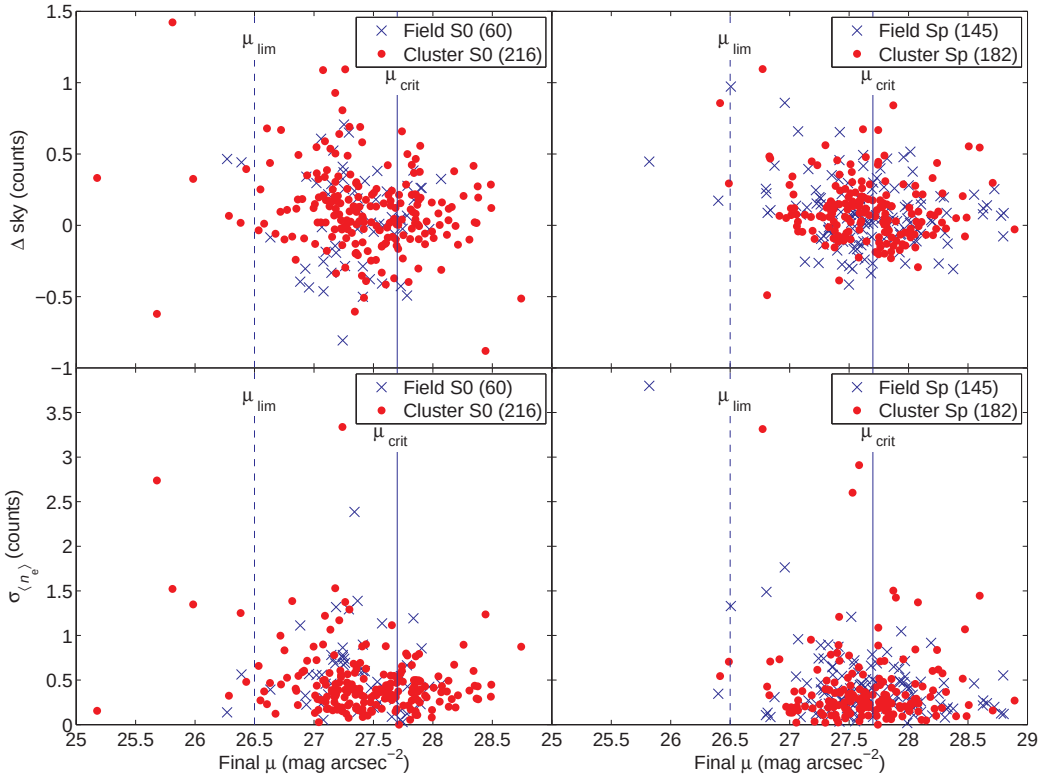

Figure 3. An evaluation of the sky subtraction for our S0 galaxies. Left-hand panels: a plot of the final surface brightness reached by the isophotal fit $\mu(r \rightarrow \infty)$ against the difference in our two sky values Δsky (top) and the corner-to-corner rms in the mean sky value for each galaxy image $\sigma_{\langle n_e \rangle}$ (bottom). Right-hand panels: a similar evaluation for the spiral galaxies from Maltby et al. (2012a). Respective sample sizes are shown in the legends.

stamps are variable and were designed to optimally contain the galaxy during the STAGES GALFIT model fits (see Gray et al. 2009, for full details)[6]. Consequently, in sampling the corners of the postage stamp we have a reasonable expectation of probing the actual sky background. These corner pixels were selected using quarter-circle wedges of side equal to 5 per cent of the smallest image dimension. We then apply our bad pixel masks to ensure only 'dark' pixels are used and obtain the mean pixel value $\langle n_e \rangle$ in each wedge. The corner-to-corner rms in these mean pixel values $\sigma_{\langle n_e \rangle}$ is then calculated in order to determine if there is any large-scale variation in the sky level across the galaxy image. In the vast majority of cases (> 90 per cent), $\sigma_{\langle n_e \rangle} < 1$ count (count $\equiv$ ACS pixel values). Finally, we obtain our sky estimate $sky_{\rm est}$ by calculating the weighted mean of $\langle n_e \rangle$ from the four corners of the image

$$sky_{\rm est} = \sum_{i=1}^{4} w_i \langle n_e \rangle_i. \quad (2)$$

The weight factor w_i is necessary due to the bad pixel masking and is given by

$$w_i = \frac{N_{i:\rm total} - N_{i:\rm masked}}{\sum_{i=1}^{4} N_{i:\rm total} - N_{i:\rm masked}}, \quad (3)$$

where $N_{i:\rm masked}$ is the number of flagged pixels and $N_{i:\rm total}$ is the total number of pixels in the respective corner wedge.

In the vast majority of cases (> 90 per cent), the agreement between the GALAPAGOS sky level $sky_{\rm gal}$ and our rough sky estimate $sky_{\rm est}$ was very good ($|\Delta sky| < 0.5$ counts, where $\Delta sky = sky_{\rm est} - sky_{\rm gal}$). Furthermore, in ~ 50 per cent of cases the agreement was within the $\pm 1\sigma$ error in $sky_{\rm gal}$ ($|\Delta sky| < 0.18$ counts; see Section 3.1). However, we need to ensure that any difference in these two sky values (Δsky), or indeed any variation in the sky level across the ACS image ($\sigma_{\langle n_e \rangle}$), will not lead to a significant oversubtraction or undersubtraction of the sky in our S0 $\mu(r)$ profiles and e.g. cause general curvature in the outer regions.

To address this issue, we compare Δsky and $\sigma_{\langle n_e \rangle}$ with the final mean surface brightness reached by the galaxy $\mu(r)$ profile $\mu_{r \rightarrow \infty}$ (see Fig. 3). In general, $\mu_{r \rightarrow \infty}$ is taken to be the mean μ after the oversubtracted $\mu(r)$ profile (-1σ sky) drops below the $\mu_{\rm crit}$ level[7]. The difference between $\mu_{r \rightarrow \infty}$ and $\mu_{\rm crit}$ (1σ above the sky) is a measure of the quality of the sky subtraction. Ideally $\mu_{r \rightarrow \infty} > \mu_{\rm crit}$, but this is not always the case due to measurement errors in the sky background. In reality, the sky subtraction is only suspect if $\mu_{r \rightarrow \infty}$ approaches the $\mu_{\rm lim}$ level (3σ above the sky). In the few cases where $\mu_{r \rightarrow \infty} < \mu_{\rm lim}$, projection effects or nearby stars are

[6] Note: the size of the postage stamps are a multiple ($2.5\times$) of the Kron (1980) radius, and therefore by definition contain $\geqslant 95$ per cent of the subject galaxy's light (Barden et al. 2012).

[7] Note: in the ~ 5 per cent of cases where the oversubtracted $\mu(r)$ does not drop below the $\mu_{\rm crit}$ level, we use the mean μ after the declining $\mu(r)$ profile levels off (i.e. enters the sky background).

known to have affected the measured $\mu(r)$ and are flagged in our analysis. If a large potential sky error (large Δsky) or a large sky variation (large $\sigma_{\langle n_e \rangle}$) were causing a significant error in our sky subtraction, one would expect a correlation between $\mu_{r\to\infty}$ and either Δsky or $\sigma_{\langle n_e \rangle}$, respectively. However, no such correlations are observed (see Fig. 3). These results suggest that cases where $\mu_{r\to\infty}$ approaches the $\mu_{\rm lim}$ level are not the consequence of a small measurement error in our GALAPAGOS sky background or small variations in the sky level across the ACS image. Therefore, we conclude that our GALAPAGOS sky values are robust and that any small sky errors are not likely to effect the outcome of this study.

To further validate this result, we perform the same tests using the sample of spiral galaxies from Maltby et al. (2012a), where no sky subtraction problems were suspected. Reassuringly, the distributions of $\mu_{r\to\infty}$ with Δsky and $\sigma_{\langle n_e \rangle}$ for these spiral galaxies are essentially the same as for our S0s (see Fig 3). Therefore, we can conclude that the GALAPAGOS sky values are adequate for this study, and that the general curvature and lack of truncations observed in our S0 $\mu(r)$ profiles appear *not* to be a manifestation of a sky subtraction error and are a real feature of our S0 galaxies.

4 PROFILE CLASSIFICATION

4.1 Profile inspection

For each S0 galaxy in our field and cluster sample, the azimuthally-averaged radial surface brightness $\mu(r)$ profile was visually inspected in order to identify potential profile breaks (inflection points in the exponential region of the μ profile). Due to the subjective nature of some profile classifications, this inspection was carried out by three independent assessors (DTM, AAS, MEG). Four possible cases were considered: i) a simple exponential profile with no break; ii) a single broken exponential either down-bending or up-bending; iii) cases with two profile breaks; and iv) no discernible exponential component (i.e. general curvature throughout the μ profile). In each case, break identification relates to the outer disc component of the galaxy $\mu(r)$ profile and does not consider the inner varying bulge component. We do not trust breaks with a break surface brightness $\mu_{\rm brk}$ fainter than the $\mu_{\rm lim}$ level ($26.5\,{\rm mag\,arcsec^{-2}}$, 3σ above the sky), as this is where break identification becomes unreliable due to the deviation of the $\mu(r)$ profiles generated by oversubtracting and undersubtracting the sky by $\pm1\sigma$. We therefore restrict our analysis to μ breaks that have $\mu_{\rm brk} < 26.5\,{\rm mag\,arcsec^{-2}}$.

In this work, we follow the same procedure as Maltby et al. (2012a) for the identification of our μ profile breaks. Therefore, our break identification is based solely on the $\mu(r)$ profiles and without direct inspection of the ACS images. As with Maltby et al. (2012a), we have chosen not to relate the $\mu(r)$ breaks to visually identified structural features because we wanted a break identification method that treated all galaxies equally, in a self-consistent manner and avoided the prejudice that image inspection could introduce. In addition to this, the aims of this work are to explore the effect of the galaxy environment on the structure of S0 galactic discs, regardless of the origins of any identified structural features. Note however, that although we use the same procedure as Maltby et al. (2012a) to identify breaks, we do not adopt their classification scheme (based on $\mu_{\rm brk} > 24\,{\rm mag\,arcsec^{-2}}$) and use the standard scheme based on the entire disc component (see Section 4.2).

If a μ profile break was identified, the radial limits of exponential regions either side of the break radius $r_{\rm brk}$ were also estimated. For the inner exponential, the inner boundary is manually selected to avoid the region dominated by the bulge component. For the outer exponential, the outer boundary is generally taken to be where the $\mu(r)$ profile reaches the critical surface brightness $\mu_{\rm crit}$ (1σ above the sky) but may be at a higher μ depending on the nature of the profile. A small manually selected transition region (non-exponential) is allowed between the exponential regions either side of the break. The break radius $r_{\rm brk}$ is defined as the mean radius of the two radial limits for this transition region.

The distributions of break surface brightness $\mu_{\rm brk}$ [$\mu(r_{\rm brk})$] for the breaks identified by the three assessors are shown in Fig. 4. The $\mu_{\rm brk}$ distributions for both one and two break cases are similar for each assessor. However, due to the subjective nature of some galaxy profile classifications, the number of galaxies with either no, one, or two breaks, varies subtly between the different assessors. To account for this, in what follows we perform parallel analysis on the breaks identified by each assessor and compare the final results.

4.2 Profile types

We classify our S0 galaxies into four main types: those classified to be Type I, Type II, or Type III depending on break features in their stellar disc; and Type c – cases with no significant exponential component (general curvature). If the galaxy has a single exponential $\mu(r)$ profile with no break it is classified as Type I. If the $\mu(r)$ profile has a down-bending break then the galaxy has a stellar disc truncation and is classified as Type II. If the $\mu(r)$ profile has an up-bending break then the galaxy has an antitruncation in the stellar disc and is classified as Type III. However, if the $\mu(r)$ profile has no discernible exponential component (general curvature throughout) then the galaxy is classified as Type c. Note that this classification scheme is based on the entire disc component and *not* on the outer disc ($\mu > 24\,{\rm mag\,arcsec^{-2}}$) as in Maltby et al. (2012a).

This classification assumes only one $\mu(r)$ break at most in the stellar disc. This is the case for ~ 95 per cent of our field and cluster S0 galaxies (see Fig. 4). In this study, we wish to consider the effect of the galaxy environment on the outer regions of S0 stellar discs. Therefore, if two breaks are present the outer break is used for classification as any effect of the environment should be stronger in the outer, fainter and more fragile break. Examples of each profile type (Type I, II, III and Type c) are shown in Fig. 5 along with their ACS images showing the break radius $r_{\rm brk}$ isophote.

4.3 Measuring scalelength and break strength

In the following section, we obtain our exponential fits by using a linear least-squares fit to the original $\mu(r)$ profile between the radial limits identified during the visual inspection (see Section 4.1).

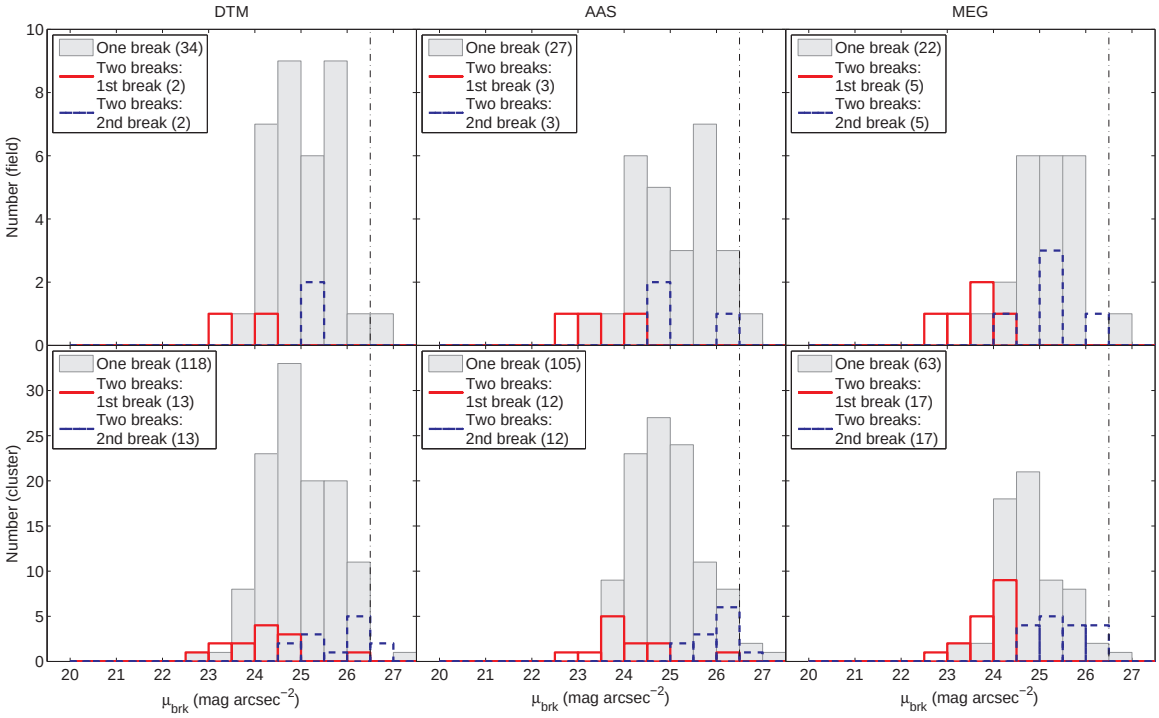

Figure 4. The distribution of break surface brightness $\mu_{\rm brk}$ for our S0 galaxies. The surface brightness at the break radius $\mu_{\rm brk}$ for field (top row) and cluster (bottom row) S0 galaxies as determined by DTM (left-hand column), AAS (centre column) and MEG (right-hand column). The distributions show galaxies with one break (grey shaded area), and both the inner (red line) and outer break (blue dashed line) of galaxies with two breaks. Respective sample sizes are shown in the legends. Systematic errors in $\mu_{\rm brk}$ due to the error in the sky subtraction are $< 0.25\,{\rm mag\,arcsec^{-2}}$. Contamination of the cluster sample by the field is < 25 per cent. Due to the subjective nature of some galaxy profile classifications, the number of galaxies with either one or two breaks varies subtly between the different assessors.

For S0 galaxies with no $\mu(r)$ profile break in their disc component (Type I, pure exponentials), we obtain the disc scalelength h from a simple exponential fit across the length of the disc component

$$h = 1.086 \times \Delta r / \Delta \mu_{\rm fit}(r), \tag{4}$$

where $\mu_{\rm fit}$ is the surface brightness from the exponential fit. For these galaxies, the mean random error in scalelength due to the exponential fitting routine is < 10 per cent and the mean systematic error in scalelength due to the error in the sky subtraction $\pm 1\sigma$ (see Section 3.1) is also < 10 per cent.

For S0 galaxies where a $\mu(r)$ profile break was observed (Type II/III), we obtain the inner/outer scalelength h from exponential fits to the stellar disc either side of the break radius $r_{\rm brk}$. The inner exponential disc extends from a radius of $r_{\rm in,min}$ to $r_{\rm in,max}$ and has a scalelength $h_{\rm in}$ given by

$$h_{\rm in} = 1.086 \times \frac{r_{\rm in,max} - r_{\rm in,min}}{\mu_{\rm fit}(r_{\rm in,max}) - \mu_{\rm fit}(r_{\rm in,min})}, \tag{5}$$

Similarly, the outer exponential disc extends from a radius of $r_{\rm out,min}$ to $r_{\rm out,max}$ and has a scalelength $h_{\rm out}$ given by

$$h_{\rm out} = 1.086 \times \frac{r_{\rm out,max} - r_{\rm out,min}}{\mu_{\rm fit}(r_{\rm out,max}) - \mu_{\rm fit}(r_{\rm out,min})}. \tag{6}$$

For these galaxies, the mean random error in scalelength due to the exponential fitting routine is < 10 per cent for $h_{\rm in}$ and < 20 per cent for $h_{\rm out}$.

In the outer regions of the surface brightness profile, negative sky-subtracted flux can occur. As surface brightness μ cannot be defined for a negative flux, these points are removed from our linear exponential fits to the $\mu(r)$ profile. However, the removal of these negative fluxes is not expected to introduce any bias on our scalelength h measurements (Maltby et al. 2012a). Some example $\mu(r)$ profiles with fitted exponential regions and overplotted break radii are shown in Fig. 5. The ACS images and $\mu(r)$ profiles for all our S0 galaxies are presented in Appendix A (on-line version only).

In order to measure the strength of our Type II/III profile breaks, we define a break strength T as the logarithm of the outer-to-inner scalelength ratio,

$$T = \log_{10} h_{\rm out}/h_{\rm in}. \tag{7}$$

A Type I galaxy (pure exponential) has no break and therefore has a break strength of $T = 0$. A Type II galaxy (down-bending break, truncation) has a smaller outer scalelength $h_{\rm out}$ with respect to its inner scalelength $h_{\rm in}$, and therefore has a negative break strength ($T < 0$). Similarly, a Type III galaxy (up-bending break, antitruncation) has a larger outer scalelength $h_{\rm out}$ with respect to its inner scalelength $h_{\rm in}$, and therefore has a positive break strength ($T > 0$). For our S0 galaxy samples, the mean random error in T due to the exponential fitting routine is $\sim \pm 0.1$ (< 20 per cent) and the mean systematic error in T due to the sky subtraction error is also $\sim \pm 0.1$.

In this study, the majority of our field S0s have a redshift $z \sim 0.23$ while our cluster S0s have $z \sim 0.167$. However, evolutionary effects are not expected to have a significant impact on our results. The break strength T of our field

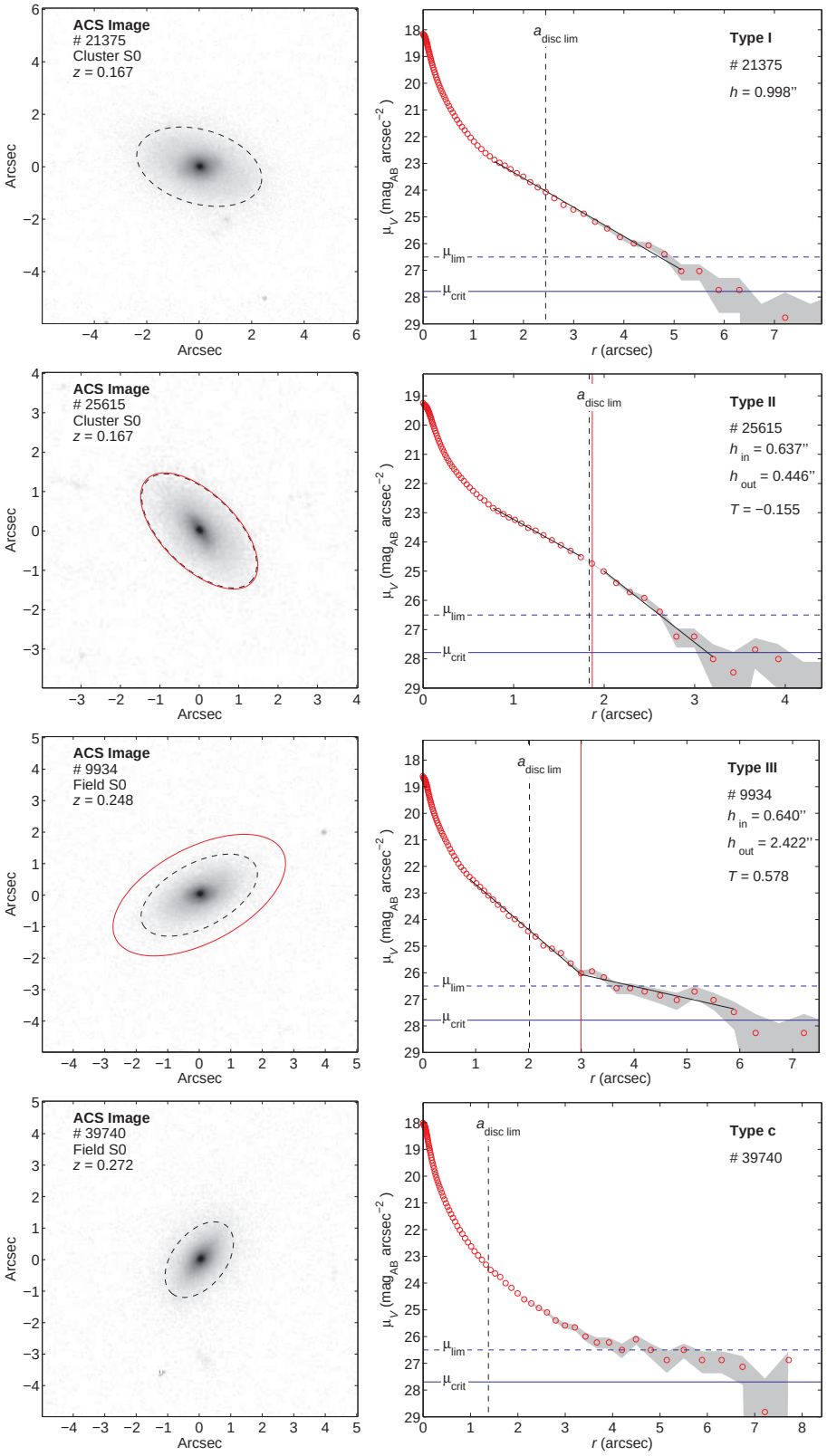

Figure 5. Examples of each class of S0 profile (DTM classification). Top to bottom: Type I, Type II, Type III and Type c (no discernible exponential component, i.e. general curvature). Left-hand panels: ACS V-band images. Right-hand panels: azimuthally-averaged V-band radial surface brightness profiles. We overplot the break radii where applicable (red solid lines) and the stellar disc limit $a_{\rm disc\,lim}$ (a visual estimate of the end of the stellar disc, black dashed line). The inner and outer scalelength, $h_{\rm in}$ and $h_{\rm out}$, respectively, and the break strength T are also shown for reference. Errors in the $\mu(r)$ profiles are for an oversubtraction and an undersubtraction of the sky by 1σ. The $\mu_{\rm crit}/\mu_{\rm lim}$ levels represent $+1\sigma/+3\sigma$ above the sky, respectively. The ACS images are in a logarithmic grey-scale. Note that in our samples, Type II S0 profiles are very rare (<5 per cent).

galaxies show no correlation with redshift and evolutionary effects on the disc scalelength h between the mean redshifts of our field and cluster samples are only ~ 5 per cent (based on the fits of Buitrago et al. 2008, for the expected size evolution of massive disc galaxies).

5 RESULTS

The frequencies of the profile classifications by each assessor (DTM, AAS, MEG) for S0 galaxies in the field and cluster environments are shown in Table 2. Profile frequencies are also shown for the low-axis-ratio ($q > 0.5$) S0 sub-sample (see Section 2.2). These profile classifications are based on single disc breaks only and in multiple break cases the outer break is used for classification. The 1σ uncertainty in the frequency/fraction of profile types δf_i ($f_i = N_i/N_{\rm tot}$) is determined using the Wilson (1927) binomial confidence interval

$$f_i \pm \delta f_i = \frac{N_i + \kappa^2/2}{N_{\rm tot} + \kappa^2} \pm \frac{\kappa\sqrt{N_{\rm tot}}}{N_{\rm tot} + \kappa^2}\sqrt{f_i(1-f_i) + \frac{\kappa^2}{4N_{\rm tot}}}, \quad (8)$$

where κ is the $100(1-\alpha/2)$th percentile of a standard normal distribution (α being the error percentile corresponding to the 1σ level; see Brown et al. 2001 for further details).

Due to the subjective nature of some profile classifications, the frequency obtained for each profile type varies subtly between the different assessors. The agreement between the assessors is generally very good, especially for Type I and II profiles. However, the agreement is slightly weaker for the frequencies of Type III and Type c (non-exponential) profiles due to the increased level of subjectivity involved in differentiating between these two profile types.

The frequencies of the profile types (Type I, II and III) are approximately the same in the field and cluster environments. For both field and cluster S0s, ~ 25 per cent have a simple exponential profile (Type I), < 5 per cent exhibit a down-bending break (truncation, Type II) and ~ 50 per cent exhibit an up-bending break (antitruncation, Type III)[8]. The frequency of profiles with no discernible exponential component (i.e. general curvature, Type c) is also approximately the same in the field and cluster environments and is ~ 20 per cent. Restricting our analysis to low inclination systems ($i < 60^\circ$, $q > 0.5$) affects our profile fractions by ~ 5 per cent but has no effect on our conclusions (see Table 2). These results suggest that the profile type of S0 galaxies is not significantly affected by the galaxy environment from the general field to the intermediate densities of the STAGES A901/2 clusters.

5.1 The absence of S0 Type II profiles

The distinct lack of disc truncations (Type II profiles) in both our field and cluster S0s is of particular interest. Type II profiles are very common in spiral galaxies, occurring in approximately 40–60 per cent of cases (Pohlen & Trujillo 2006; Erwin et al. 2008; Gutiérrez et al. 2011). Therefore, it seems whatever process transforms spiral galaxies into S0s may well erase these truncations from their $\mu(r)$ profiles. This result is in partial agreement with a similar result reported recently by Erwin et al. (2012). Using a sample of ~ 70 field and cluster S0 galaxies, Erwin et al. (2012) find no Type II S0s in the cluster environment but a Type II fraction of ~ 30 per cent for their field S0s. Therefore, our Type II S0 fractions are in perfect agreement with Erwin et al. (2012) for the cluster environment, but differ significantly for the field. The origin of this disagreement is uncertain but may be related to the low fraction of barred S0s in our field sample (see Table 1).

In order to explore this issue, it is important to note that Type II profiles can be further classified into two main subtypes depending on their potential origin – Type II-CT and Type II-OLR (Pohlen & Trujillo 2006; Erwin et al. 2008). Type-II-CT profiles (classical truncations) are cases where the truncation appears to be related to a radial star formation threshold, whereas Type II-OLR profiles are cases where the presence of a bar appears to have introduced a Type II feature related to the outer Lindblad resonance (OLR). In our field sample, the bar fraction is only ~ 10 per cent (see Table 1). This contrasts with a field bar fraction of > 50 per cent in Erwin et al. (2012). Consequently, the lower fraction of barred S0s (and hence Type II-OLR profiles) in our field sample could easily be the origin of the observed differences between our results and those of Erwin et al. (2012).

An explanation for the lack of Type II profiles in our S0s can be hypothesised by considering their potential origin. For classical truncations (Type II-CT), current theories suggest that their formation is via a radial star formation threshold and the outward scattering of inner disc stars to regions beyond this threshold (i.e. break radius $r_{\rm brk}$; e.g. Debattista et al. 2006). In these cases, the outer disc should be populated by old stars as these are the ones that have had enough time to make the disc migration. The discovery that the stellar mass surface density $\Sigma^{M_*}(r)$ profiles of late-type Type II galaxies tend to be purely exponential (Bakos et al. 2008; Martínez-Serrano et al. 2009) supports this scenario and suggests that Type II $\mu(r)$ breaks are *not* related to the stellar mass distribution but due to a radial change in the age of the stellar population. Assuming this formation scenario, and an inside-out growth for the inner disc [i.e. negative age(r) gradient], when star formation is suppressed throughout the galaxy (e.g. via gas stripping) the age of the stellar population in the 'break region' will gradually increase. As a result, the relative difference in stellar population age between the break region and inner/outer discs will decrease and the mass-to-light ratio (M/L) across the $\mu(r)$ break will converge. Consequently, the μ break will get weaker and may even disappear. For Type II-OLR profiles, the μ break is expected to be related to a resonance phenomenon and therefore the above scenario does not hold. However, Erwin et al. (2012) suggest that the depletion/removal of gas from a barred galaxy would cause a weakening of the OLR effect and may weaken or remove the Type II-OLR break from the $\mu(r)$ profile. Considering these theories, and since spiral galaxies are thought to transform into S0s via the depletion/removal of gas and the subsequent termination of star formation (e.g. Aragón-Salamanca et al. 2006), it seems natural to expect Type II $\mu(r)$ breaks to be weaker/rarer in S0s compared to spiral galaxies.

[8] Note: in Section 7.2, we find that a significant fraction of our Type III S0 profiles (up to ~ 50 per cent) may actually be related to light from an extended bulge component and not an antitruncated stellar disc.

Table 2. The frequency of profile types for S0 galaxies in the field and cluster environments and for the three independent assessors (DTM, AAS, MEG). Profile frequencies are also shown for the low-axis-ratio ($q > 0.5$) S0 sub-sample. Percentage errors are calculated using equation 8.

Assessor	Disc profile types			Curvature	Unclassified
	Type I	Type II	Type III	Type c	
Field S0 galaxies					
DTM	18 (30 ± 6 %)	1 (2^{+3}_{-1} %)	34 (57 ± 6 %)	5 (8^{+4}_{-3} %)	2 (3^{+3}_{-2} %)
AAS	18 (30 ± 6 %)	0 ($0 + 2$ %)	29 (48 ± 6 %)	13 (22^{+6}_{-5} %)	0 ($0 + 2$ %)
MEG	17 (28^{+6}_{-5} %)	0 ($0 + 2$ %)	26 (43 ± 6 %)	14 (23^{+6}_{-5} %)	3 (5^{+4}_{-2} %)
Cluster S0 galaxies					
DTM	43 (20 ± 3 %)	8 (4^{+2}_{-1} %)	122 (56 ± 3 %)	37 (17^{+3}_{-2} %)	6 (3 ± 1 %)
AAS	58 (27 ± 3 %)	5 (2 ± 1 %)	109 (50 ± 3 %)	41 (19 ± 3 %)	3 (1 ± 1 %)
MEG	56 (26 ± 3 %)	2 (1 ± 1 %)	77 (36 ± 3 %)	68 (31 ± 3 %)	13 (6^{+2}_{-1} %)
Field S0 galaxies ($q > 0.5$)					
DTM	11 (31^{+8}_{-7} %)	1 (3^{+4}_{-2} %)	20 (56 ± 8 %)	3 (8^{+6}_{-4} %)	1 (3^{+4}_{-2} %)
AAS	13 (36^{+8}_{-7} %)	0 ($0 + 3$ %)	14 (39 ± 8 %)	9 (25^{+8}_{-6} %)	0 ($0 + 3$ %)
MEG	14 (39 ± 8 %)	0 ($0 + 3$ %)	13 (36^{+8}_{-7} %)	8 (22^{+8}_{-6} %)	1 (3^{+4}_{-2} %)
Cluster S0 galaxies ($q > 0.5$)					
DTM	37 (27 ± 4 %)	6 (4^{+2}_{-1} %)	71 (52 ± 4 %)	17 (12 ± 3 %)	6 (4^{+2}_{-1} %)
AAS	47 (34 ± 4 %)	3 (2^{+2}_{-1} %)	60 (44 ± 4 %)	24 (18 ± 3 %)	3 (2^{+2}_{-1} %)
MEG	45 (33 ± 4 %)	2 (1 ± 1 %)	40 (29 ± 4 %)	38 (28 ± 4 %)	12 (9^{+3}_{-2} %)

5.2 S0: pure exponential discs (Type I)

For S0s where no $\mu(r)$ break was identified (Type I), we compare the scalelength h distributions in the field and cluster environments to see whether there is any evidence for an environmental dependence on the scalelength h (see Fig. 6). In these comparisons, our scalelengths h were transformed into intrinsic linear scales using the fixed cluster redshift ($z_{\rm cl} = 0.167$) for our cluster S0s and the COMBO-17 photo-z estimate for our field S0s. Therefore, photo-z errors only propagate into the intrinsic scalelengths of our field galaxies and not our cluster galaxies. The mean error in h associated with this photo-z error is < 10 per cent (i.e. the error in the distance to the galaxy; Maltby et al. 2010).

For our $\mu(r)$ profiles, the error in the sky background (see Section 3.1) can have a significant effect on both our scalelength h and break strength T measurements, especially at large radii where the $\mu(r)$ profile approaches the critical surface brightness $\mu_{\rm crit}$ ($27.7\,{\rm mag\,arcsec^{-2}}$, 1σ above the sky). However, for any particular galaxy the sky subtraction error can be taken to be approximately constant across the length of the $\mu(r)$ profile. Therefore, we can account for this error by performing parallel analyses for when the sky background is oversubtracted and undersubtracted by $\pm 1\sigma$ (± 0.18 counts). For our Type I S0s, the mean error in h due to the sky subtraction error is $\sim \pm 0.3\,{\rm kpc}$ (< 10 per cent). Random errors in h due to the exponential fitting routine are also typically < 10 per cent (see Section 4.3). We also perform parallel analyses on the Type I samples generated by the three assessors (DTM, AAS, MEG) in order to account for the subjective nature of the profile classifications and compare the final results.

In all cases (all parallel analyses), we observe no clear difference between the distributions of scalelength h for our Type I S0s in the field and cluster environments (see Fig. 6). This is also the case when considering only the low-axis-ratio ($q > 0.5$) S0 sub-sample. In order to test the significance of these results, we construct scalelength h cumulative distribution functions (CDFs, see Fig. 6) for our Type I S0 samples and perform Kolmogorov–Smirnov (K–S) tests between corresponding samples from the field and cluster environments. These K–S tests are used in order to obtain the probability $p_{\rm (field/cluster)}$ that the field and cluster Type I S0 samples are *not* drawn from the same continuous h distributions. The results of these K–S tests, for both the full S0 sample and the low-axis-ratio ($q > 0.5$) S0 sub-sample, are shown in Table 3.

In this study, we only consider an environmental effect on the Type I scalelength h to be significant if K–S tests yield a 2σ level probability for $p_{\rm (field/cluster)}$. However, $p_{\rm (field/cluster)}$ is below the 2σ level for each assessor and for when the sky background is oversubtracted and undersubtracted by $\pm 1\sigma$ (see Table 3). This is also the case for the low-axis-ratio S0 sub-sample. Therefore, we find no evidence to suggest that the disc scalelength h of our Type I S0s is dependent on the galaxy environment. This result is also robust to the error in the sky subtraction and the subjective nature of the profile classifications.

5.3 S0: broken exponential discs (Type II/III)

For S0 galaxies where a $\mu(r)$ break was identified[9] (Type II/III), we compare the break surface brightness $\mu_{\rm brk}$ and break strength T distributions in the field and cluster environments. These comparisons are presented in Section 5.3.1 and Section 5.3.2, respectively.

[9] Note: if two $\mu(r)$ breaks are identified in any one galaxy, the outer break is used in the analysis.

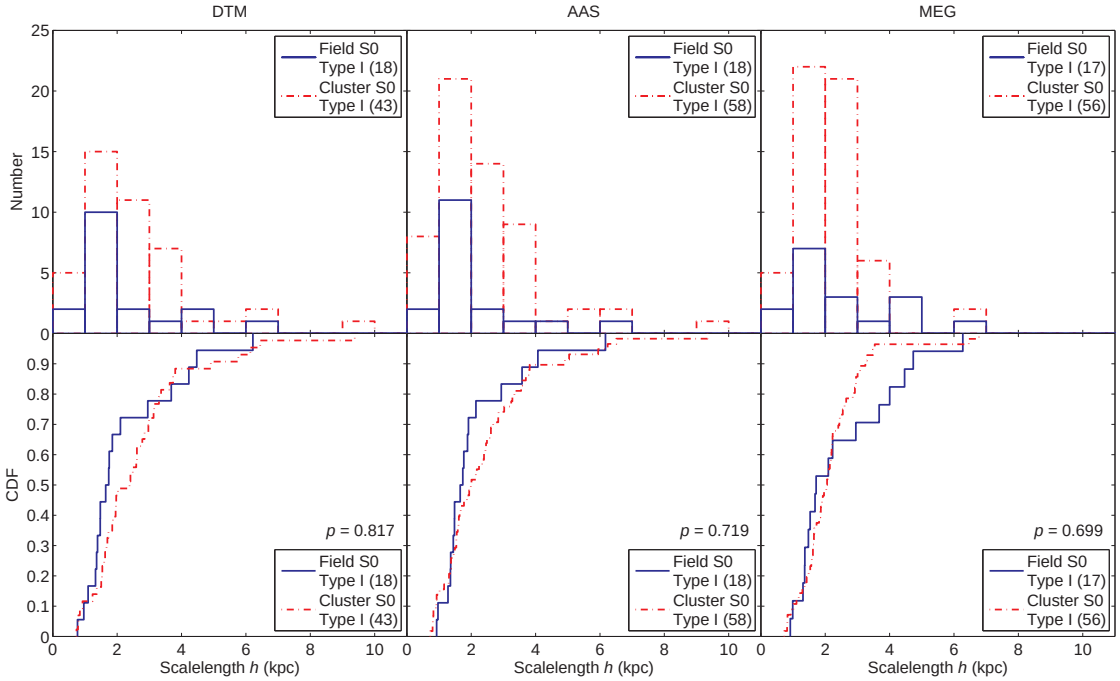

Figure 6. Comparing Type I disc scalelength h distributions in different environments for S0 galaxies (full sample). Top row: scalelength h distributions for Type I S0 galaxies in the field (blue line) and cluster (red dashed line) environment as classified by DTM (left-hand panel), AAS (centre panel) and MEG (right-hand panel). Bottom row: the corresponding scalelength h CDFs showing the probability p that compared samples are *not* drawn from the same continuous h distributions in the bottom right of each plot. Respective sample sizes are shown in the legends. Random errors in scalelength are typically < 10 per cent. Systematic errors in scalelength due to the error in the sky subtraction are also typically < 10 per cent. Contamination of the cluster sample by the field is < 25 per cent. We find no significant difference between the CDFs in each environment and no evidence to suggest that the scalelengths h of our Type I S0 galaxies are *not* drawn from the same continuous h distributions.

Table 3. The K–S test results for Type I and Type III S0s as classified by DTM, AAS and MEG. Results are also shown for the low-axis-ratio ($q > 0.5$) S0 sub-sample. K–S tests give the probability $p_{(\mathrm{field/cluster})}$ that the respective field and cluster samples are *not* drawn from the same h distributions for Type I S0s and μ_{brk}/T distributions for Type III S0s. Results are also shown for when the sky is oversubtracted and undersubtracted by $\pm 1\sigma$. We find no environmental dependence on the structural properties of the stellar disc (h, μ_{brk}, T) in our S0 galaxies.

	S0 sample $p_{(\mathrm{field/cluster})}$			S0 sub-sample ($q > 0.5$) $p_{(\mathrm{field/cluster})}$		
Sky subtraction	Under (-1σ)	Nominal	Over ($+1\sigma$)	Under (-1σ)	Nominal	Over ($+1\sigma$)
S0: Type I (h)						
DTM	0.811	0.817	0.822	0.572	0.572	0.787
AAS	0.755	0.719	0.804	0.370	0.327	0.344
MEG	0.589	0.699	0.621	0.566	0.497	0.383
S0: Type III (μ_{brk})						
DTM	0.536	0.504	0.682	0.589	0.398	0.352
AAS	0.099	0.206	0.121	0.523	0.477	0.222
MEG	0.902	0.812	0.937	0.983	0.984	0.981
S0: Type III (T)						
DTM	0.732	0.226	0.357	0.226	0.062	0.331
AAS	0.909	0.864	0.436	0.523	0.381	0.551
MEG	0.925	0.821	0.154	0.877	0.761	0.083

5.3.1 Break surface brightness $\mu_{\rm brk}$

Certain physical processes inherent to galaxy evolution and related to the galaxy environment could potentially affect the position of $\mu(r)$ breaks. For example in the cluster environment, tidal/ram-pressure stripping (Gunn & Gott 1972; Faber 1973) could remove gas from the stellar disc, causing star formation to cease in the outer regions as the gas density drops below the star-formation threshold. This would cause the outer regions to gradually fade as the stellar population ages. For classical truncations (Type II-CT), gas (and hence star formation) is not expected to occur beyond the break radius $r_{\rm brk}$ (see Section 5.1); and therefore such gas processes should only act on the inner disc. This may result in $\mu_{\rm brk}$ (i.e. the end of the starforming inner disc) evolving to a slightly brighter μ in the cluster environment. However, for Type III profiles the outer disc is thought to form via the displacement of disc stars in a minor merger (e.g. Younger et al. 2007); and therefore gas (and star formation) may still be prevalent beyond $r_{\rm brk}$. In these cases, cluster processes (e.g. ram-pressure stripping) may result in a general fading across the break and cause $\mu_{\rm brk}$ to evolve to a fainter μ in the cluster environment (although the exact effect will be dependent on the relative fading of the inner and outer discs). These are just two possible scenarios (there may be many others), and illustrate the potential for an effect of the environment on break surface brightness $\mu_{\rm brk}$. Consequently, the comparison of $\mu_{\rm brk}$ distributions for Type II/III galaxies could provide some insight into the effect of the galaxy environment on galactic discs.

Therefore, for S0 galaxies where a Type II/III $\mu(r)$ break was identified, we compare the break surface brightness $\mu_{\rm brk}$ distributions in the field and cluster environments in order to see if there is any evidence for an environmental dependence on $\mu_{\rm brk}$. However, in such comparisons, it is important to remember that Type II breaks generally occur at a brighter $\mu_{\rm brk}$ than Type III breaks and that environmental processes may affect these breaks in different ways. Therefore, in order to ensure our S0 $\mu_{\rm brk}$ comparisons are fair, we only compare the $\mu_{\rm brk}$ distributions for our field/cluster S0 Type III galaxies (see Fig. 7). Note that we cannot compare the $\mu_{\rm brk}$ distributions for Type II profiles since they are very rare in our S0 galaxies (see Table 2). Analogous parallel analyses and statistical tests are performed as in our Type I profile analysis (see Section 5.2) and the results of the K–S tests, for both the full S0 sample and the low-axis-ratio ($q > 0.5$) S0 sub-sample, are shown in Table 3.

For our Type III S0 galaxies, in all cases (all assessor samples and sky versions), we observe no significant difference between the $\mu_{\rm brk}$ distributions in the field and cluster environments. The probability $p_{\rm (field/cluster)}$ is below the 2σ level in each case. For our S0 ($q > 0.5$) sub-sample, in a few cases the probability $p_{\rm (field/cluster)}$ is above the 2σ level (MEG results, see Table 3). However, this result is not consistent between the different assessors (i.e. robust to the subjective nature of the profile classifications). Therefore, we conclude that there is no evidence to suggest that the break surface brightness $\mu_{\rm brk}$ of our S0s is dependent on the galaxy environment. However, we stress that this result may suffer from low number statistics and a larger field sample may yield different results. We also note that for our Type III S0 galaxies, a significant fraction (up to ~ 50 per cent) may actually be related to light from an extended bulge component and not due to an antitruncated stellar disc (see Section 7.2). In such cases, the suppression of star-formation in the disc may cause $\mu_{\rm brk}$ to evolve to a brighter μ. This is due to the inner star-forming disc fading more quickly than the old extended bulge component ($r > r_{\rm brk}$), once star formation has ceased. This could potentially mask an environmental effect in our Type III $\mu_{\rm brk}$ comparisons. We shall return to this issue in Section 6.4.1.

For our Type III S0s, we also perform an analogous comparison using the break radius $r_{\rm brk}$ distributions in the field and cluster environments ($r_{\rm brk}$ in units of the effective radius of the GALFIT Sérsic model). As with our $\mu_{\rm brk}$ analysis, we find no significant difference between the $r_{\rm brk}$ distributions of our Type III S0s in the field and cluster environments. However, we note that the Sérsic effective radius is not an ideal unit to measure the break radius $r_{\rm brk}$ and a non-parameterized effective radius may yield more robust results.

5.3.2 Break strength T

For our Type III S0s, we also compare the break strength T distributions in the field and cluster environments in order to see if there is any evidence for an environmental dependence on break strength T (see Fig. 8). Note that we only compare the T distributions for our Type III S0s since i) the effect of environment may be different for Type II/III profiles; and ii) Type II profiles are very rare in our S0 galaxies. Similar parallel analyses and statistical tests are also carried out as in our S0 Type I profile analysis (Section 5.2). The mean error in T due to the sky subtraction error is ± 0.1 and random errors in T due to exponential fitting routine are also typically ± 0.1 (see Section 4.3). The results of the K–S tests, for both the full S0 sample and the low-axis-ratio ($q > 0.5$) S0 sub-sample, are shown in Table 3.

In all cases (all assessor samples and sky versions), we observe no significant difference between the break strength T distributions in the field and cluster environments. The probability $p_{\rm (field/cluster)}$ is below the 2σ level in each case. Therefore, we find no evidence to suggest that the break strength T of our Type III S0 galaxies is dependent on the galaxy environment. This result is also robust to the error in the sky subtraction and the subjective nature of the profile classifications.

6 THE STRUCTURE OF GALACTIC DISCS IN SPIRAL AND S0 GALAXIES

In this study, we have so far explored the effect of the galaxy environment on the structure of galactic discs in STAGES S0 galaxies. This work is analogous to our companion study (Maltby et al. 2012a), which explores the effect of the galaxy environment on the structure of galactic discs in STAGES *spiral* galaxies. For spiral galaxies, Maltby et al. (2012a) found no evidence to suggest that their $\mu(r)$ profiles were affected by the galaxy environment. Both the scalelength h and break strength T of their spiral galaxies showed no evidence for an environmental dependence from the general field to the intermediate galaxy densities probed by the STAGES survey. Therefore, our conclusion that there

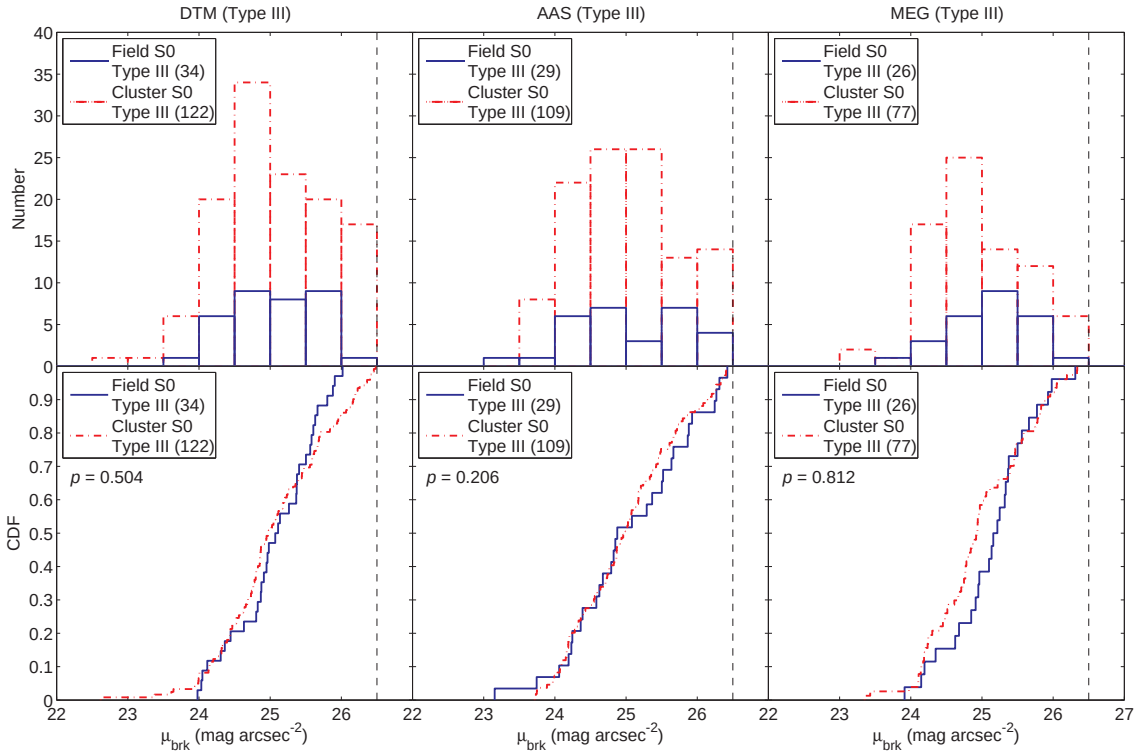

Figure 7. Comparing break surface brightness $\mu_{\rm brk}$ distributions in different environments for Type III S0 galaxies (full sample). Format as in Fig. 6. Respective sample sizes are shown in the legends. Contamination of the cluster sample by the field is < 25 per cent. We find no significant difference between the CDFs in each environment and no evidence to suggest that the $\mu_{\rm brk}$ of our Type III S0s are *not* drawn from the same continuous $\mu_{\rm brk}$ distributions.

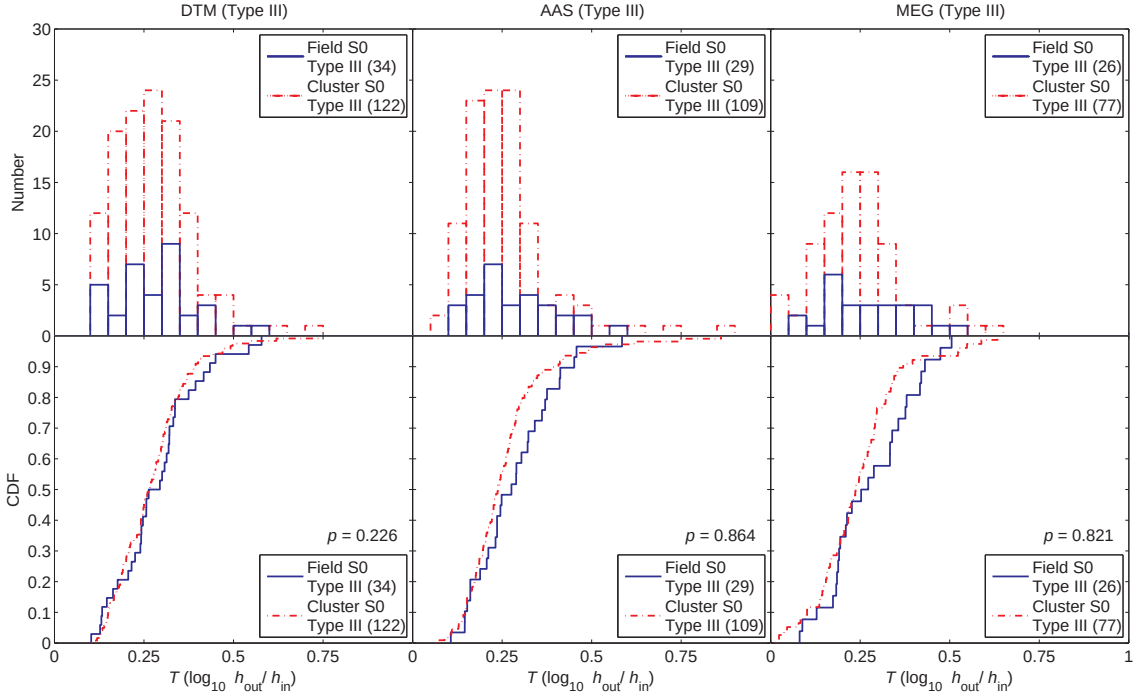

Figure 8. Comparing break strength T ($\log_{10} h_{\rm out}/h_{\rm in}$) distributions in different environments for Type III S0 galaxies (full sample). Format as in Fig. 6. Respective sample sizes are shown in the legends. Random errors in T are typically < 0.1. Systematic errors in T due to the error in the sky subtraction are also $\sim \pm 0.1$. Contamination of the cluster sample by the field is < 25 per cent. We find no significant difference between the CDFs in each environment and no evidence to suggest that the break strengths T of our Type III S0s are *not* drawn from the same continuous T distributions.

is no evidence for an effect of the galaxy environment on the structure of S0 galactic discs is in qualitative agreement with the conclusions presented in Maltby et al. (2012a) for spiral galaxies.

In this section, we compare our results for S0s with those for spiral galaxies from Maltby et al. (2012a) in order to assess the effect of galaxy morphology on the structure of galactic discs. Such comparisons of disc structure (e.g. profile type, scalelength h, break strength T, break surface brightness $\mu_{\rm brk}$) between different Hubble-type morphologies are a useful tool in exploring the potential evolutionary link between spiral and S0 galaxies.

However, in these comparisons it is important to note that the break classification scheme used by Maltby et al. (2012a) differs from the one used in this work. In Maltby et al. (2012a), break classification is based on the outer stellar disc ($\mu > 24\,{\rm mag\,arcsec^{-2}}$), while in this work the entire disc component is used. Fortunately, Maltby et al. (2012a) identify breaks across the entire disc component prior to their classification and also identify Type I profiles based on the entire disc. Therefore, their Type I scalelength h and $\mu_{\rm brk}$ distributions are not limited by surface brightness and can be directly compared with the results of this work (see Sections 6.3 and 6.4.1). However, for break strength T the situation is different because Maltby et al. (2012a) only performed these measurements on Type II/III profiles in the outer stellar disc ($\mu_{\rm brk} > 24\,{\rm mag\,arcsec^{-2}}$), cases which they classify as Type $\rm II_o/III_o$ profiles (o – outer). Consequently, when we compare our S0 break strength T distributions with those for spiral galaxies from Maltby et al. (2012a), we also limit our S0 breaks by $\mu_{\rm brk}$ to allow for a fair comparison (see Section 6.4.2).

6.1 Spiral/S0: galaxy samples

Both this work and Maltby et al. (2012a) use the same parent sample of morphologically classified galaxies in STAGES from which to draw their samples (see Maltby et al. 2010). Both works also perform analogous $\mu(r)$ profile fitting and break identification (see Section 4.1). Maltby et al. (2012a) use a large, mass-limited ($M_* > 10^9\,{\rm M_\odot}$), visually classified (Sa–Sdm) sample of 327 face-on to intermediately inclined ($i < 60^\circ$) spiral galaxies from both the field and cluster environments (145 field and 182 cluster spirals). In this work, our S0 sample selection is analogous to this spiral selection except for the lack of an inclination i cut (see Section 2.1). Therefore, in order to allow for a fair comparison of these spiral and S0 galaxies, we use our low-axis-ratio ($i < 60^\circ$, $q > 0.5$) S0 sub-sample of 173 S0s (36 field and 137 cluster) in all our spiral/S0 comparisons (see Section 2.2).

6.2 Profile type (Type I, II and III)

Previous works (e.g. Pohlen & Trujillo 2006; Erwin et al. 2008; Gutiérrez et al. 2011) have found that for spiral galaxies the distribution of profile types I:II:III is approximately 20:50:30 ±10 per cent. This is also true for Maltby et al. (2012a) if their spiral $\mu(r)$ profiles are re-classified based on the entire disc (see Section 1). However, in this work we find that for S0s, $\sim$ 25 per cent are Type I, $<$ 5 per cent are Type II, $\sim$ 50 per cent are Type III and $\sim$ 20 per cent have no discernible exponential component (see Section 5, Table 2). In comparing the profile types (disc structure) of these spiral/S0 galaxies, the most striking difference is the lack of truncations (Type II profiles) in our S0s compared to their abundance in spiral galaxies. Therefore, it seems whatever mechanism transforms spiral galaxies into S0s may well erase these Type II features from the galaxy $\mu(r)$ profiles. In the case of classical truncations (Type II-CT), recent studies suggest that the Type II profile is related to a radial change in the age of the stellar population throughout the disc, with the outer disc being populated by old stars and an inside-out growth for the inner disc (Debattista et al. 2006; Bakos et al. 2008; Martínez-Serrano et al. 2009). Consequently, the absence of Type II-CT profiles in our S0s may actually be a natural consequence of an ageing stellar population in the 'break region' as the spirals transform into S0s (see Section 5, for a full explanation). For bar-related truncations (Type II-OLR), the depletion/removal of galactic gas should weaken the OLR effect and may also result in the weakening/removal of the Type II feature as spirals transform into S0s (Erwin et al. 2012).

Another observation is that Type III profiles seem to be significantly more frequent in S0s than in spiral galaxies. This suggests a continuation of the observed trend for spiral galaxies where Type III profiles become more frequent with progressively earlier Hubble types (e.g. Pohlen & Trujillo 2006; Maltby et al. 2012a). Since Type III profiles are thought to form via minor mergers, this trend is consistent with a minor merger scenario for the formation of S0 galaxies. However, in Section 7.2 we find that for our Type III S0s, a significant fraction (potentially up to $\sim$ 50 per cent) may actually be related to light from an extended bulge component and not due to an antitruncated stellar disc. This is in contrast to spiral galaxies where the vast majority of Type III profiles appear to be genuine antitruncated discs (Maltby et al. 2012b). Consequently, the fraction of genuine antitruncated discs may actually be lower in S0s than in spiral galaxies. This could be due to the fading inner/outer disc causing $\mu_{\rm brk}$ to drop below the level of the bulge μ profile (or sky background) as some spirals evolve into S0s.

6.3 Spiral/S0: pure exponential discs (Type I)

For spiral/S0 galaxies where no disc $\mu(r)$ break was identified (Type I), we compare the scalelength h distributions for spiral and S0 morphologies (see Fig. 9). These comparisons are independent of the galaxy environment (our field and cluster samples are combined) and allow for an assessment of whether the scalelength h of the stellar disc is affected by the Hubble-type morphology. Similar parallel analyses are also carried out as in previous tests.

In most cases (most parallel analyses), we observe no clear difference between the scalelength h distributions for our Type I spiral and S0 galaxies (see Fig. 9). In order to test the significance of these results we construct scalelength h CDFs for our Type I spiral/S0 samples and perform K–S tests in order to obtain the probability $p_{\rm (spiral/S0)}$ that they are *not* drawn from the same continuous h distributions. The results of these K–S tests are presented in Table 4.

In most cases (most assessor samples and sky versions), the probability $p_{\rm (spiral/S0)}$ is below the 2σ level. However, in a few cases the probability $p_{\rm (spiral/S0)}$ is above the 2σ level

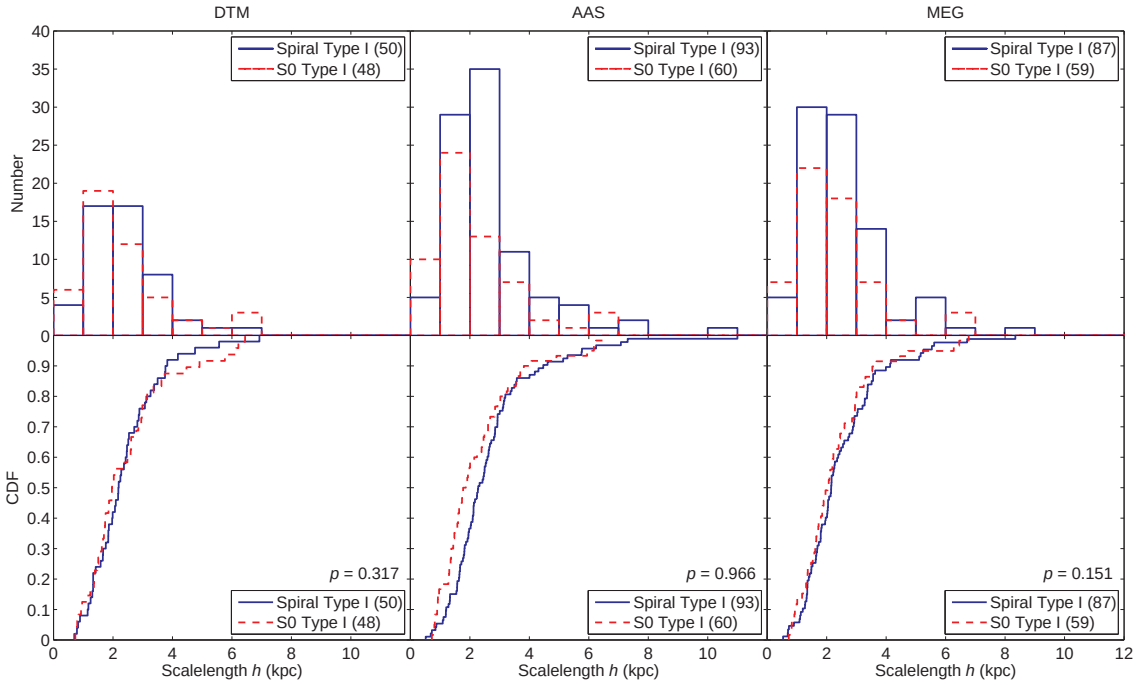

Figure 9. Comparing the disc scalelength h distributions for different Hubble-type morphologies. Top row: scalelength h distributions for spiral (blue line) and S0 (red dashed line) Type I galaxies as classified by DTM (left-hand panel), AAS (centre panel), and MEG (right-hand panel). Bottom row: the corresponding scalelength h CDFs showing the probability p that compared samples are *not* drawn from the same continuous h distributions in the bottom right of each plot. Respective sample sizes are shown in the legends. Random errors in scalelength are typically < 10 per cent. Systematic errors in scalelength h due to the error in the sky subtraction are also typically < 10 per cent. We find no significant difference between the CDFs for each morphology and no evidence to suggest that the disc scalelength h of our Type I galaxies are *not* drawn from the same continuous h distributions.

(AAS results, see Table 4). As these high significance results are not robust to the subjective nature of the profile classifications, we conclude that there is no evidence to suggest that the scalelength h of our Type I galaxies is significantly affected by the Hubble-type morphology.

6.4 Spiral/S0: broken exponential discs (Type II/III)

For spiral/S0 galaxies where a $\mu(r)$ break was identified[10] (Type II/III), we compare both the break surface brightness $\mu_{\rm brk}$ and break strength T distributions for our spiral and S0 galaxies. These comparisons are presented in Section 6.4.1 and Section 6.4.2, respectively. In these comparisons, it is important to note that for our spiral galaxies (taken from Maltby et al. 2012a), the $\mu_{\rm brk}$ distribution is for breaks identified across the entire disc, whereas the T distribution is for breaks from the outer disc only ($\mu > 24\,{\rm mag\,arcsec^{-2}}$).

6.4.1 Break surface brightness $\mu_{\rm brk}$

The physical processes that drive the morphology–density relation (Dressler 1980) and the transformation of spiral galaxies into S0s are not well understood. Certain mechanisms inherent to the cluster environment could be responsible, e.g. ram-pressure stripping of the interstellar medium, mergers and harassment (Gunn & Gott 1972; Icke 1985; Moore et al. 1996). However, the existence of S0s in the general field implies that either cluster processes are not ultimately responsible, or that S0s can form via alternative processes in different environments. For example, it could be the case that cluster S0s form from in-falling spirals via the tidal/ram-pressure stripping of interstellar gas, while field S0s are simply the faded remnants of field spirals.

For these mechanisms, the processes causing star formation to be quenched and the subsequent morphological transformation could have a distinct effect on the $\mu_{\rm brk}$ of any $\mu(r)$ break that was present (see Section 5.3.1). For example, in a Type III profile the suppression of star formation could cause $\mu_{\rm brk}$ to evolve to a fainter μ as spirals evolve into S0s. Consequently, the comparison of $\mu_{\rm brk}$ distributions for spiral and S0 Type II/III galaxies could provide some insight into the potential evolutionary links between them.

Therefore, for spiral/S0 galaxies where a $\mu(r)$ break was identified (Type II/III), we compare the $\mu_{\rm brk}$ distributions between field/cluster spiral and S0 galaxies. In such comparisons it is important to remember that Type II breaks generally occur at a brighter $\mu_{\rm brk}$ than Type III breaks. For our Type II/III spirals, ~ 50 per cent are Type III (classification based on the entire stellar disc), while our S0s are almost exclusively (> 95 per cent) Type III. Therefore, to ensure our spiral/S0 $\mu_{\rm brk}$ comparisons are fair, we only compare the $\mu_{\rm brk}$ distributions for our field/cluster spiral and S0 Type III galaxies (see Fig 10). Similar parallel analyses and

[10] Note: if two $\mu(r)$ breaks are identified in any one galaxy, the outer break is used in the analysis.

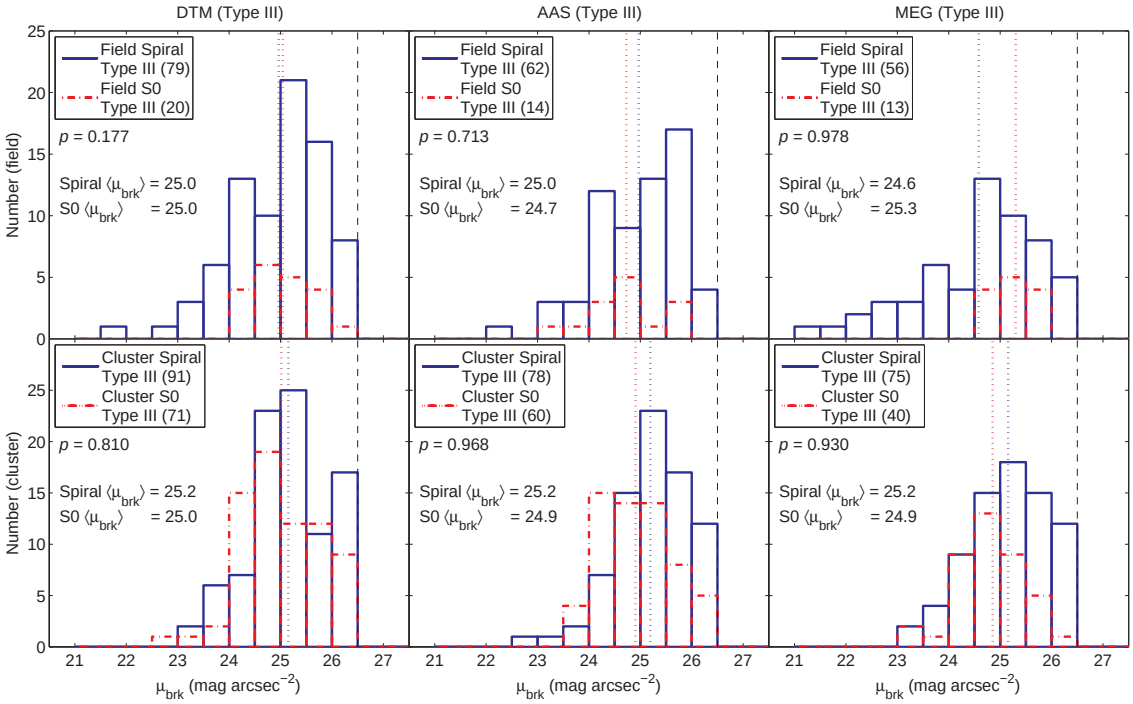

Figure 10. The break surface brightness $\mu_{\rm brk}$ distributions for Type III spiral and S0 galaxies in different environments. The $\mu_{\rm brk}$ distributions for field (top row) and cluster (bottom row) galaxies as determined by DTM (left-hand column), AAS (centre column) and MEG (right-hand column). The distributions show spiral galaxies (blue line), and S0 galaxies (red dashed line). The mean $\mu_{\rm brk}$ for field/cluster spirals (blue dotted line) and S0s (red dotted line) are also shown for reference. Respective sample sizes are shown in the legends. Contamination of the cluster sample by the field is < 25 per cent.

statistical tests (between corresponding spiral and S0 samples) are carried out as in previous tests.

For our cluster spiral/S0 comparison, in most cases (most assessor samples) we observe no significant difference between the $\mu_{\rm brk}$ distributions for spiral and S0 galaxies. The probability $p_{\rm (spiral/S0)}$ is below the 2σ level in most cases. However, for one assessor (AAS) the significance of a morphological dependence is above the 2σ level. We also note that for all assessors, the mean $\mu_{\rm brk}$ for S0s ($24.9\,{\rm mag\,arcsec^{-2}}$) is brighter than that of spiral galaxies ($25.2\,{\rm mag\,arcsec^{-2}}$). However, since this result is inconclusive we deduce that there is no evidence to suggest that $\mu_{\rm brk}$ in the cluster environment is dependent on the galaxy morphology.

For our field spiral/S0 comparison, we also observe no significant difference between the spiral/S0 $\mu_{\rm brk}$ distributions in the majority of cases (i.e. $p_{\rm (spiral/S0)} < 2\sigma$). For one assessor (MEG), the significance of a morphological dependence is above the 2σ level, but this may be due to low number statistics. It is interesting that for all assessors, the spiral $\mu(r)$ breaks reach to a brighter $\mu_{\rm brk}$ than the S0 $\mu(r)$ breaks. This would be consistent with the hypothesis that field S0s are the faded remnants of field spirals. However, since this result is based on low number statistics we conclude that there is no evidence to suggest that $\mu_{\rm brk}$ in the field is dependent on the galaxy morphology. Further investigation with a larger sample of field S0s is needed to suitably address this issue and may yield more conclusive evidence.

In these $\mu_{\rm brk}$ comparisons, it is also important to note that for our Type III S0s a significant fraction (possibly up to 50 per cent) may actually be related to light from an extended bulge component and not due to an antitruncated stellar disc (see Section 7.2). In such cases, the suppression of star-formation in the disc may cause $\mu_{\rm brk}$ to evolve to a brighter μ. This is due to the inner star-forming disc fading more quickly than the old extended bulge component ($r > r_{\rm brk}$), once star formation has ceased. In contrast, for spiral galaxies the vast majority of our Type III profiles appear to be genuine antitruncated discs (Maltby et al. 2012b). Consequently, a significant fraction of our Type III S0s may not have evolved from a Type III spiral galaxy, potentially leading to a masking of any morphological trends in our $\mu_{\rm brk}$ comparisons. A robust method for differentiating between genuine antitruncated discs and those caused by an extended bulge is needed to address this problem (see Section 7.2).

Similar analyses were also performed using the break radius $r_{\rm brk}$ distributions ($r_{\rm brk}$ in units of the GALFIT Sérsic model effective radius). As with our $\mu_{\rm brk}$ analysis, no significant differences or trends were observed for $r_{\rm brk}$ in field/cluster spiral and S0 galaxies. However, we note that the Sérsic effective radius is not an ideal unit to measure the break radius $r_{\rm brk}$ and a non-parameterized effective radius may yield more robust results.

6.4.2 Break strength T

In Maltby et al. (2012a), break strength T measurements were only performed on $\mu(r)$ breaks in the outer regions of the stellar disc $\mu_{\rm brk} > 24\,{\rm mag\,arcsec^{-2}}$ (their criteria for selecting intrinsically similar outer breaks in spiral galax-

Table 4. The K–S test results for Type I and Type II_o/III_o galaxies as classified by DTM, AAS and MEG. K–S tests give the probability $p_{(spiral/S0)}$ that the respective spiral and S0 samples are *not* drawn from the same continuous h distributions for Type I galaxies, and T distributions for Type II_o/III_o galaxies. Results are also shown for when the sky is oversubtracted and undersubtracted by $\pm1\sigma$.

	$p_{(spiral/S0)}$		
Sky subtraction	Under (-1σ)	Nominal	Over ($+1\sigma$)
Type I (h)			
DTM	0.293	0.317	0.477
AAS	0.966	0.966	0.981
MEG	0.056	0.151	0.346
Type II/III (T)			
DTM	0.996	0.988	0.989
AAS	0.996	0.969	0.997
MEG	0.983	0.957	0.972
Type III (T)			
DTM	0.9998	0.9994	0.9999
AAS	0.99999	0.99997	0.995
MEG	0.99992	0.9997	0.975

ies). They refer to these 'outer disc' breaks as Type II_o and Type III_o profiles. Therefore, in order to allow for a fair comparison between the break strength T distributions of our S0s and the spiral galaxies of Maltby et al. (2012a), we also need to limit our S0 break strength T distributions by break surface brightness ($\mu_{brk} > 24\,mag\,arcsec^{-2}$). However, since the vast majority (~ 95 per cent) of our S0 Type II/III profiles have $\mu_{brk} > 24\,mag\,arcsec^{-2}$ anyway, this has little effect on our S0 break strength T distributions (see Fig. 7).

Fig. 11 shows a comparison of the break strength T distributions for our Type II_o/III_o spiral/S0 galaxies. These comparisons are independent of the galaxy environment (our field and cluster samples are combined) and allow for an assessment of whether the break strength T of the stellar disc is affected by the Hubble-type morphology. Similar parallel analyses and statistical tests are also carried out as in previous tests and the results of the K–S tests are presented in Table 4.

In all cases (all assessor samples and sky versions), we observe a *significant difference* between the T distributions for spiral and S0 Type II_o/III_o galaxies. The probability $p_{(spiral/S0)}$ is above the 3σ level in each case. Additionally, the break strength T distribution of our S0s has a much smaller variance (S0 $\sigma_T \sim 0.15$) compared to that of our spiral galaxies (spiral $\sigma_T \sim 0.4$). These results suggest that both Type II_o and Type III_o features in S0s are weaker (smaller $|T|$) than in spiral galaxies.

However, it is possible that the high significance of this result could be driven by the lack of Type II profiles in our S0s. Therefore, we repeat our analysis using the break strength T distributions for just our Type III_o galaxies (see Fig. 12). The results of the K–S tests are presented in Table 4. In all cases (all assessor samples and sky versions), we still observe a significant difference between the T distributions for our spiral and S0 Type III_o galaxies. The probability $p_{(spiral/S0)}$ is above the 3σ level in each case. Also, the break strength T distribution of our Type III_o S0s has a much smaller variance and mean (S0s: $\sigma_T \sim 0.13$, $\langle T \rangle \sim 0.28$) compared to that of our spiral Type III_o galaxies (spirals: $\sigma_T \sim 0.3$, $\langle T \rangle \sim 0.4$).

Therefore, we conclude that there is some evidence to suggest that the break strength T of our Type II_o/III_o galaxies is dependent on the galaxy morphology, with $\mu(r)$ breaks in S0s being generally weaker (smaller $|T|$) than those of spiral galaxies. This result is also robust to the error in the sky subtraction and the subjective nature of the profile classifications. Additionally, since the S0 T distribution is much tighter than that of spiral galaxies the potential contamination of our Type III_o S0s by non-genuine stellar disc antitruncations (i.e. extended bulge components; see Section 7) has no effect on this conclusion.

We propose that this result is consistent with current theories on the origin of Type II/III profiles. For classical truncations (Type II-CT), the $\mu(r)$ break is thought to be related to a radial variation in the age of the stellar population, with the outer disc being populated by old stars (Debattista et al. 2006; Bakos et al. 2008; Martínez-Serrano et al. 2009). In this scenario, once the galaxy has depleted its gas supply, star formation will cease in the 'break region' causing it to gradually fade due to the ageing of the stellar population. This would lead to a weakening of the Type II break strength T (see Section 5.1). For bar-related truncations (Type II-OLR), the depletion/removal of galactic gas should weaken the OLR effect and may also result in a weakening of the Type II break strength T (Erwin et al. 2012). For Type III galaxies, further radial mixing related to the suspected minor-merger history could be responsible for the weakening of the Type III feature in S0 galaxies.

7 ANTITRUNCATED SURFACE BRIGHTNESS PROFILES: BULGE OR DISC RELATED?

Antitruncated (Type III) surface brightness $\mu(r)$ profiles have a broken exponential with a shallower region beyond the break radius r_{brk} (i.e. up-bending break, see Fig. 5). However, the excess light at large radii is not necessarily related to an outer exponential disc and could also be associated with an extended spheroidal bulge or halo. This idea was first postulated by Erwin et al. (2005), who suggest that Type III profiles can be separated into two distinct sub-classes depending on whether the outer profile $r > r_{brk}$ is dominated by a stellar disc (Type III-d) or a spheroidal component (Type III-s).

In Erwin et al. (2005), they propose that antitruncations with a smooth gradual transition and outer isophotes that are progressively rounder than that of the main disc, suggest an inclined disc embedded in a more spheroidal outer region such as an extended bulge or halo (i.e. Type III-s). Using this 'ellipse' method, previous works (Erwin et al. 2005, 2008; Gutiérrez et al. 2011) have found that ~ 40 per cent of their Type III profiles are Type III-s. However, the ellipse method is limited for face-on discs and cases where the outer/inner disc may have different orientations and axis ratios. In these cases, an alternative method would be to use bulge–disc (B–D) decomposition (e.g. Allen et al. 2006) to determine the contribution of the two main structural com-

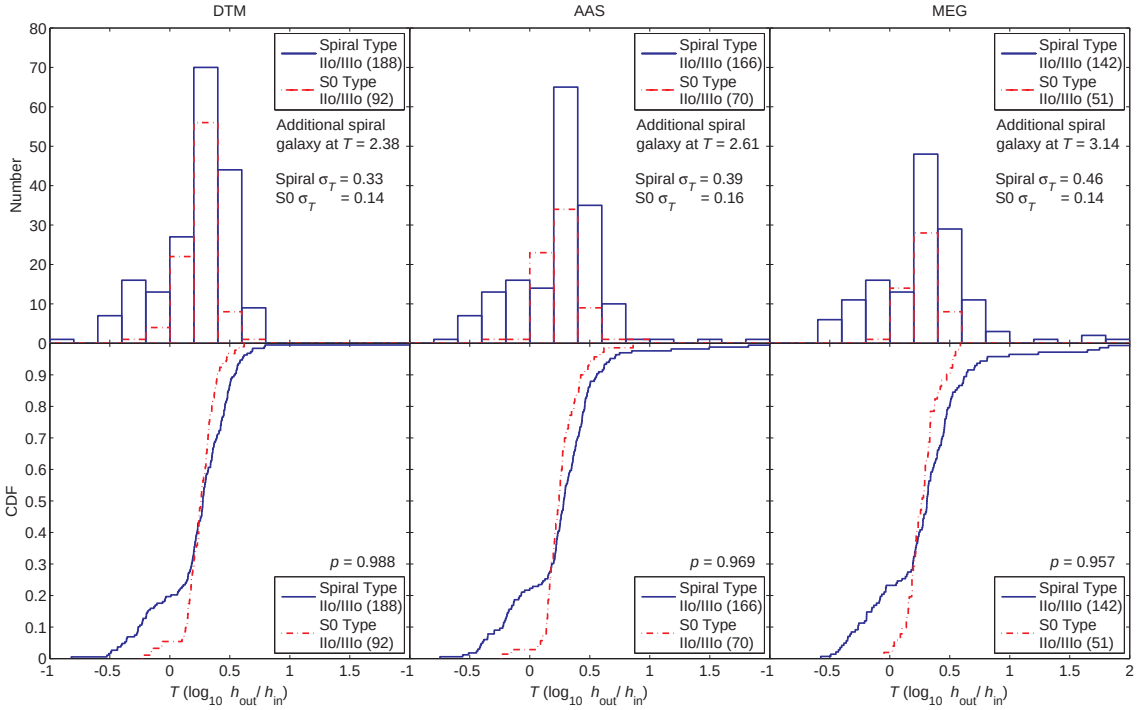

Figure 11. Comparing break strength T ($\log_{10} h_{\rm out}/h_{\rm in}$) distributions for spiral and S0 galaxies. Top row: break strength T distributions for spiral (blue line) and S0 (red dashed line) Type $\rm II_o/III_o$ galaxies as classified by DTM (left-hand column), AAS (centre column) and MEG (right-hand column). Bottom row: the corresponding break strength T CDFs showing the probability p that compared samples are *not* drawn from the same continuous T distributions in the bottom right of each plot. Respective sample sizes are shown in the legends. Random errors in T are $\sim \pm 0.1$. Systematic errors in T due to the sky subtraction error are also $\sim \pm 0.1$. Contamination of the cluster sample by the field is < 25 per cent. We find a significant ($> 3\sigma$) difference between the T CDFs for spiral and S0 galaxies.

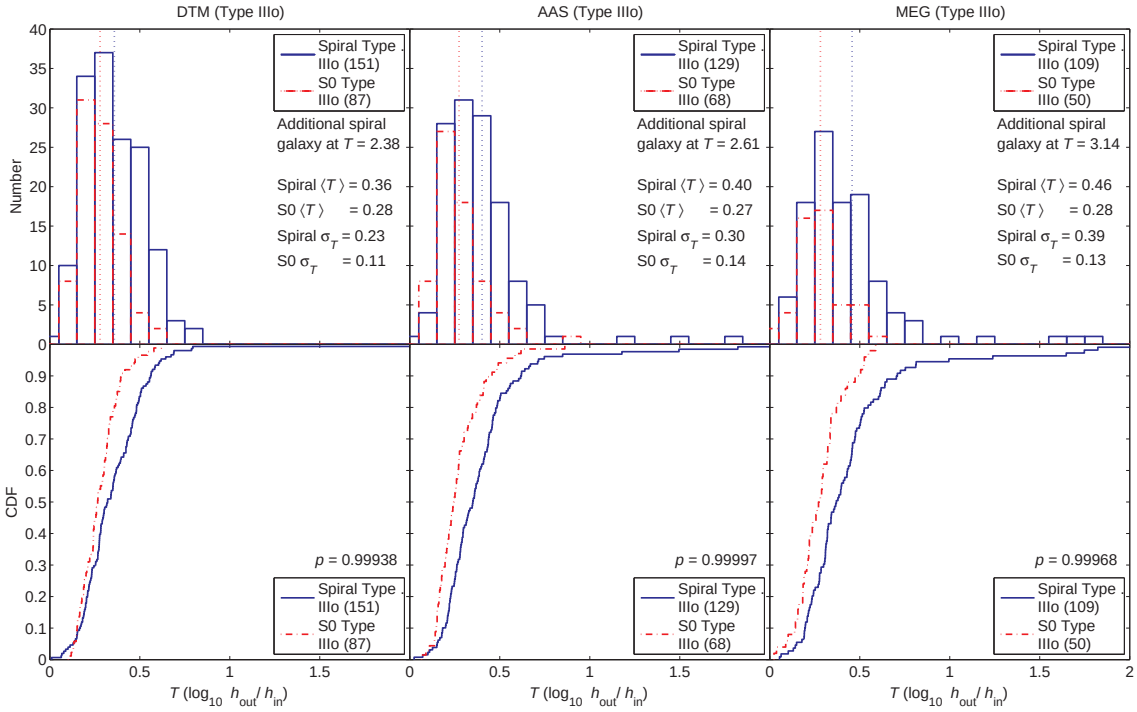

Figure 12. Comparing break strength T ($\log_{10} h_{\rm out}/h_{\rm in}$) distributions for Type $\rm III_o$ spiral and S0 galaxies. Figure the same as Fig. 11 but for Type $\rm III_o$ galaxies only. We find a significant ($> 3\sigma$) difference between the T CDFs for spiral and S0 galaxies. The mean T for spirals (blue dotted line) and S0s (red dotted line) are also shown for reference. Respective sample sizes are shown in the legend.

ponents (bulge and disc) to the galaxy's light distribution and should provide more robust results.

In this section, we explore the nature of Type III $\mu(r)$ profiles in S0 galaxies, using bulge–disc (B–D) decomposition in order to determine the maximum possible contribution of bulge light in their outer regions ($r > r_{\rm brk}$). Using these analyses, we determine the maximum fraction of Type III S0s for which the excess light at large radii could be caused or affected by the spheroidal component (i.e. Type III-s). This study complements our previous work, Maltby et al. (2012b), which presents an analogous study using Type III *spiral* galaxies. We review the findings of Maltby et al. (2012b) in Section 7.1, before presenting the results for our S0s in Section 7.2.

7.1 Antitruncations in spiral galaxies

Maltby et al. (2012b) explore the nature of Type III $\mu(r)$ profiles in spiral galaxies and determine the *maximum* fraction of Type III spirals for which the excess light at large radii could be caused or affected by the spheroidal component (i.e. Type III-s). They achieve this by comparing azimuthally-averaged radial $\mu(r)$ profiles with analytical B–D decompositions (de Vaucouleurs, $r^{1/4}$ bulge plus single exponential disc) for 78 Type III spirals, and determine the *maximum* possible contribution of bulge light in the outer regions ($r > r_{\rm brk}$) of each galaxy. B–D decomposition was performed on all 327 spirals defined in Maltby et al. (2012a) (see Section 6.1) and their Type III spirals were drawn from this parent sample[11].

Using these comparisons, Maltby et al. (2012b) find that for the majority of their Type III spirals ($\sim$ 70 per cent), the excess light beyond the break radius $r_{\rm brk}$ is clearly related to an outer shallow disc (Type III-d). In addition, they also find a further $\sim$ 15 per cent which are also Type III-d, but where the contamination by extended bulge light affects the measured properties of the outer, disc-dominated region (e.g. $\mu_{\rm brk}$, outer scalelength). For the remaining Type III spirals ($\sim$ 15 per cent), the excess light at $r > r_{\rm brk}$ could potentially be attributed to the bulge profile (Type III-s).

In considering these results it is important to note that the methodology adopted by Maltby et al. (2012b) has two main drawbacks: i) in a two-component B–D decomposition, an outer antitruncated disc, bar feature or outer halo could cause the bulge profile to be constrained; and ii) in many cases the bulge component may be not be de Vaucouleurs in nature (i.e. less concentrated – pseudo bulge). These issues lead to an over-estimation of bulge light in the outer regions of some galaxies. This naturally enhances the fraction of Type III-s profiles in Maltby et al. (2012b), which therefore represents an upper limit to the fraction of genuine Type III-s profiles in their Type III spirals. Adding more degrees of freedom to their galaxy model (more components; Sérsic bulge profile) would address this issue. However, degeneracy issues would affect the reliability of their B–D decompositions and could lead to many Type III-s profiles being misclassified. Consequently, in assessing the potential impact of the bulge component on the outer regions of the galaxy, it becomes desirable to consider the *maximum* possible effect (i.e. a de Vaucouleurs, $r^{1/4}$ bulge). Taking this into consideration, Maltby et al. (2012b) conclude that in the vast majority of cases Type III profiles in spiral galaxies are indeed a true disc phenomenon.

[11] Note: in Maltby et al. (2012b), B–D decomposition failed for two spiral galaxies, hence a total sample of 325 spirals was used.

7.2 Antitruncations in S0 galaxies

We explore the nature of Type III $\mu(r)$ profiles in our S0s by using an analogous method to that used for spiral galaxies in Maltby et al. (2012b) (see Section 7.1). We therefore determine the *maximum* fraction of Type III S0s for which the excess light at large radii could be caused or affected by the spheroidal component.

For this study, we use the low-axis-ratio sample of 173 S0s defined in Section 2.2 and used throughout Section 6 (hereafter refered to as the total S0 sample). However, we remove five of these galaxies for which B–D decomposition fails (probably due to contamination from a nearby star or companion galaxy; $N_{\rm tot} = 168$). We also use the disc profile classifications from Section 5 to obtain a robust S0 sub-sample of 39 Type III $\mu(r)$ profiles (i.e. where classifications from the three independent assessors were in agreement). We use both this Type III sub-sample and the total S0 sample in this study.

7.2.1 Bulge–disc decompositions

For each S0 galaxy in our total sample, we perform a two-dimensional B–D decomposition based on a two-component galaxy model comprising a de Vaucouleurs ($r^{1/4}$) bulge and a single exponential disc. Decompositions were carried out on the STAGES V-band imaging using the GALFIT code (Peng et al. 2002) and the method of Hoyos et al. (2012) adapted to perform two-component fits. Several measurable properties are produced for each galaxy including position [x,y], effective radii, total magnitudes, axial ratios, position angles for the bulge and disc components and a sky-level estimation.

In this work, it is important to note that our B–D decompositions are not intended to yield the actual bulge components of our S0 galaxies. Instead the intention is to obtain the *maximum* possible contribution a bulge profile can give to the light in the outer regions of a galaxy. This is the motivation behind adopting a de Vaucouleurs ($r^{1/4}$) profile for our bulge components instead of a free Sérsic profile (see Section 7.1, for further details). However, we acknowledge that many of our S0s will have less concentrated bulge profiles (i.e. pseudo bulges) and that our B–D decompositions will (by design) over-estimate the bulge light in the outer regions of some galaxies.

B–D decomposition can be sensitive to the initial conditions used to search the B–D parameter space (e.g. initial estimate for bulge-to-disc ratio B/D). Therefore, we perform two runs of the B–D decomposition with different initial conditions taken from the two extremes: one run starting from a bulge-dominated system ($B/D = 9$) and the other run starting from a disc-dominated system ($B/D = 1/9$). Comparison of these runs (hereafter Run 1 and Run 2, respectively) allows for an assessment of the uniqueness/stability of B–D decomposition on a galaxy–galaxy basis.

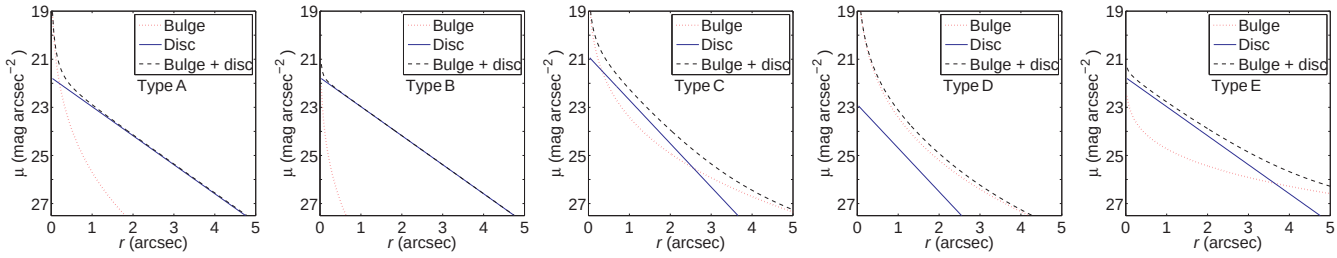

Figure 13. B–D profile types. Left to right: Type A – 'classical' system; Type B – disc-dominated system; Type C – bulge-dominated at small/large radii but disc-dominated at intermediate radii; Type D – bulge-dominated system; Type E – probable 'constrained' outer bulge (caused by an outer shallow disc).

In the vast majority of cases ($\sim$ 90 per cent) the results were effectively the same, $\sim$ 85 per cent being exactly the same and $\sim$ 5 per cent showing only minor differences. In only a few cases ($<$ 5 per cent) were the decompositions catastrophically unstable with Run 1/2 yielding both bulge- and disc-dominated systems. The remaining cases ($\sim$ 5 per cent), showed moderate instabilities great enough to affect the assessment of bulge light in the outer regions of the galaxy. The unstable solutions are mainly driven by differences in the sky level determined during the decomposition. However, the overall conclusions of this study are not affected by these unstable solutions. The stability fractions quoted are the same for both the total sample and the Type III sub-sample.

7.2.2 B–D profile types

B–D decompositions using a de Vaucouleurs ($r^{1/4}$) bulge plus an exponential disc can be classified into four distinct profile types (e.g. Maltby et al. 2012b), see Fig. 13.

(1) *Type A:* 'classical' system. The bulge profile dominates in the central regions, while the disc profile dominates at larger radii. The bulge/disc profiles cross only once.
(2) *Type B:* disc-dominated system. The disc profile dominates at all radii, with a weak contribution from the bulge profile in centre. The bulge/disc profiles never cross.
(3) *Type C:* the bulge profile dominates at small/large radii, but the disc profile dominates at intermediate radii.
(4) *Type D:* bulge-dominated system. The bulge profile dominates at all radii with a weak underlying disc component. The bulge/disc profiles never cross[12].

In addition to these profile types, a further class (hereafter Type E) is also observed where the disc profile dominates in the central regions, but the bulge profile dominates at larger radii. In such cases, it is probable that an outer antitruncated disc has incorrectly affected the bulge profile fit. Consequently, for Type E profiles B–D decomposition is not a true representation of the galaxy at large radii and in reality these galaxies probably have Type B compositions (or similar). Analogous constraints may also occur in some Type D profiles.

Fig. 14(a) shows the distribution of B–D profile types for both the total S0 sample and Type III sub-sample.

[12] Note: capital letters are used in our B–D profile types to avoid confusion with the other classification schemes used in this paper.

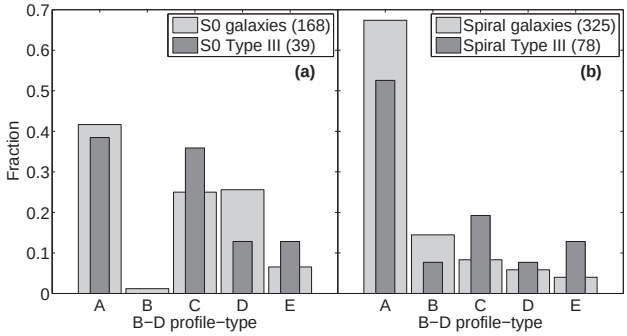

Figure 14. The distribution of B–D profile types in disc galaxies. Left-hand panel: the distribution for S0 galaxies (from Run 1). Distributions are presented for the total S0 sample (light grey) and the Type III S0 sub-sample (dark grey). Right-hand panel: analogous distributions for the spiral galaxies presented in Maltby et al. (2012b). Respective sample sizes are shown in the legends.

Comparing these distributions, we find that the fraction of Type C/E profiles is greater in the Type III sub-sample. This is expected from the nature of Type C/E profiles (i.e. excess light at large radii, see Fig. 13). A similar trend is also observed in the distribution of B–D profile types for *spiral* galaxies in Maltby et al. (2012b) [see Fig. 14(b)]. However, a comparison of the B–D profile type distributions between spiral and S0 galaxies shows some distinct differences. The fraction of disc-dominated B–D profile types (Type A/B) is much larger in spiral galaxies compared with S0s. Conversely, the fraction of bulge-dominated B–D profile types (Type C/D) is much larger in S0s compared with spiral galaxies. Therefore, these distributions indicate that on average S0s have a higher B/D than spiral galaxies, an observation that has also been reported previously by several authors (e.g. Simien & de Vaucouleurs 1986; Laurikainen et al. 2010).

We expand on this result by comparing the bulge PA (from B–D decomposition) with a visual estimate for the PA of the outer galactic region (i.e. PA of the outer stellar disc used in our fixed-ellipse fits, see Section 3). Fig. 15 shows these comparisons for both our sample of S0s and the spiral galaxies from Maltby et al. (2012a,b). For spiral galaxies, there is no obvious correlation between the PA of the bulge and the outer galactic region. This indicates that our visual estimates are not related to the inner bulge and are indeed probing an outer disc component. Additionally, since

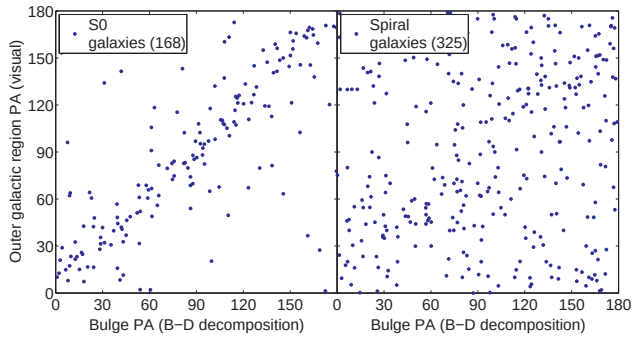

Figure 15. A comparison of the bulge PA (from B–D decomposition) with a visual estimate for the PA of the outer galactic regions (i.e. outer stellar disc, see Section 3) for both our S0 galaxies (left-hand panel) and the spiral galaxies from Maltby et al. (2012b) (right-hand panel). Respective sample sizes are shown in the legends.

galactic discs are essentially axisymmetric (a consequence of rotational motion), the misalignment between the bulge and the disc also suggests a triaxial (non-axisymmetric) nature for the bulges of our spiral galaxies (see e.g. Bertola et al. 1991). In contrast, for S0 galaxies there is a significant correlation between the PA of the bulge and the outer galactic region. This alignment between the bulge and the disc component implies a bulge that is axisymmetric (oblate) in nature for many of our S0 galaxies. However, this alignment also suggests the possibility that for some of our S0s, the visual estimates are actually probing the outer regions of the bulge component (and not the stellar disc). This result is consistent with the observation that S0s tend to have a higher B/D than spiral galaxies. Considering the high fraction of bulge-dominated B–D profiles (Type C/D) in our S0s, this is not surprising (see Fig. 14). However, more importantly, this result clearly indicates that light from the spheroidal (bulge) component potentially contributes a significant amount of light to the outer regions of some S0 galaxies. Consequently, bulge light may account for more Type III profiles in S0s than observed for spiral galaxies in Maltby et al. (2012b). We explore this issue in further detail in the following section.

7.2.3 Measured surface brightness $\mu(r)$ profiles

For each S0 galaxy, we also obtain new azimuthally-averaged radial $\mu(r)$ profiles from the STAGES *HST*/ACS V-band imaging. We achieve this using a similar methodology to that described in Section 3, but with two minor differences:

(i) in the fixed-parameter fits (fixed centre, ellipticity e and position angle PA), we use the galaxy centre determined from our B–D decomposition. As in previous sections, the e and PA used are for the outer stellar disc (see Section 3);

(ii) the necessary sky subtraction is performed using the sky-level estimates generated during B–D decomposition. Note: these sky values sometimes differ slightly from those of Gray et al. (2009) used throughout Sections 3–6.

Analogous fixed-parameter fits (using the same e and PA, i.e. the same isophotes) are also carried out on the disc-residual images (ACS image minus bulge-only model) resulting in a measured μ profile for the disc component $\mu_{\rm disc}(r)$. We also obtain azimuthally-averaged radial μ profiles for the decomposed B–D model using the same fixed-parameter ellipses (isophotes) as in the other profiles. This results in separate analytical radial μ profiles for both the bulge- and disc-model along the semimajor axis of the elliptical isophotes (i.e. outer stellar disc).

For our Type III S0s, we compare these measured $\mu(r)$ profiles with the model μ profiles from B–D decomposition in order to determine the *maximum* contribution of bulge light in the outer regions of the galaxy ($r > r_{\rm brk}$)[13]. Using an analogous scheme to that presented in Maltby et al. (2012b), we find that bulge light in the outer profile ($r > r_{\rm brk}$) either had:

(i) *little or no contribution* ($\sim$ 45 per cent): for all Type A/B profiles the bulge contributes virtually no light at $r > r_{\rm brk}$ and in some Type C/E profiles the contribution is negligible. This can be determined by inspection of the measured disc-residual profile $\mu_{\rm disc}(r)$ and assessing if the properties of the outer profile/break ($r_{\rm brk}$, $\mu_{\rm brk}$, scalelength) have been affected with respect to the sky-subtraction error. For our Type III S0s, these cases are entirely comprised of Type A profiles. No Type B profiles are observed in our Type III S0 galaxies.

(ii) *minor contribution* ($\sim$ 10 per cent): the majority of these cases are Type C profiles (with one exception which is Type E). The amount contributed is enough to affect the outer profile causing $\mu_{\rm brk}$ and the outer scalelength to be different in the disc-residual profile $\mu_{\rm disc}(r)$. However, the antitruncation remains present.

(iii) *major contribution* ($\sim$ 45 per cent): the bulge contributes the majority of the light at $r > r_{\rm brk}$. For these cases, one quarter are Type D, one quarter are Type E, and the remaining half are Type C (where the antitruncation can be entirely accounted for by bulge light, see Fig. 16 for one such an example).

These results suggest that for only about a half of Type III S0s, the excess light beyond the break radius $r_{\rm brk}$ is related to an outer shallow disc (Type III-d). For the remaining cases, the excess light at $r > r_{\rm brk}$ could be attributed to a bulge profile (Type III-s). More importantly, for these latter cases a considerable fraction ($\sim$ 20 per cent of the Type III S0 sub-sample) exhibit profiles where the bulge profile extends beyond a dominant disc (Type C) and causes an antitruncation in the $\mu(r)$ profile.

However, it is important to note that our adopted methodology does have two main drawbacks: i) in a two-component B-D decomposition an outer antitruncated disc, bar feature or outer halo could cause the bulge profile to be contrained; and ii) in many cases the bulge component may not be de Vaucouleurs in nature (i.e. less concentrated - pseudo bulge). These issues lead to an over-estimation of bulge light in the outer regions of some galaxies (see Section 7.1 and 7.2.1, for the justification of this methodology). This naturally enhances the fraction of Type III-s profiles, which therefore represents an upper limit to the fraction of

[13] Note: due to our B–D decomposition using a de Vaucouleurs, $r^{1/4}$ bulge, the model bulge profile often over-estimates the contribution of bulge light in the outer regions of the $\mu(r)$ profile.

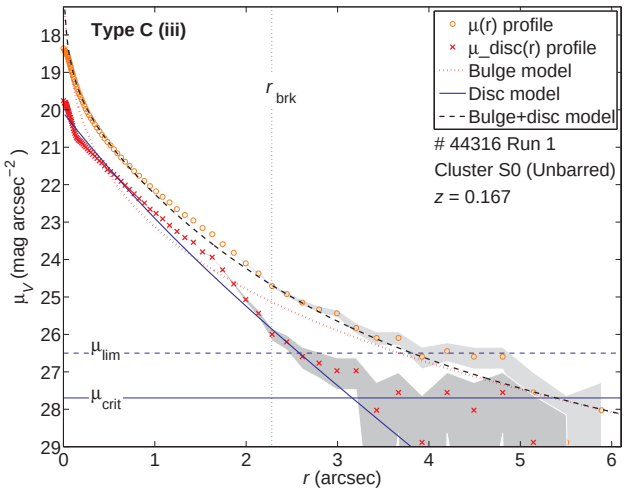

Figure 16. A common example of a bulge profile causing an anti-truncation in an S0 $\mu(r)$ profile (break radius $r_{\rm brk}$). The bulge (red dotted line), disc (blue line), and bulge + disc (black dashed line) profiles from B–D decomposition are overplotted on the measured $\mu(r)$ profile (red circles). The disc-residual $\mu_{\rm disc}(r)$ profile (measured μ profile minus bulge-only model, red crosses) shows no anti-truncation. Errors in $\mu(r)/\mu_{\rm disc}(r)$ are for an oversubtraction and an undersubtraction of the sky by 1σ. The $\mu_{\rm crit}/\mu_{\rm lim}$ levels represent $+1\sigma/+3\sigma$ above the sky, respectively.

genuine Type III-s profiles in our Type III S0s. Due to this fact, this method is unsuitable for removing Type III-s profiles from our Type III analysis in Sections 5 and 6.

With respect to these results, we conclude that bulge light is an important component in the $\mu(r)$ profiles of some S0 galaxies at large radii and that antitruncations in S0s are frequently caused by either the bulge or disc component. This is in sharp contrast to the conclusion of our analogous study for spiral galaxies, Maltby et al. (2012b), where in the vast majority of cases Type III profiles appear to be a true disc phenomenon.

7.3 Implications for the formation of S0 galaxies

Various mechanisms have been suggested to explain the transformation of spiral galaxies into S0s. However, these mechanisms generally require some type of interaction that causes a quenching of star formation and the subsequent passive evolution of the spiral galaxy into an S0 (see e.g. Aragón-Salamanca et al. 2006). The nature of this interaction could be directly related to the gaseous component, e.g. tidal/ram-pressure stripping of the inter-stellar medium (Gunn & Gott 1972; Faber 1973) or the removal of the outer gas halo (starvation; Larson et al. 1980). Alternatively, the interaction could be related to minor mergers which trigger starbursts that deplete the gas supply throughout the disc (e.g. Mihos & Hernquist 1994).

Regardless of the precise mechanism, the transition of a spiral galaxy into an S0 is expected to have a distinct effect on the B/D. For example, the suppression of star formation in the stellar disc (e.g. by gas stripping) would cause the disc component to gradually fade as the stellar population ages and the B/D to increase. However, the degree to which the disc fades in this scenario is currently uncertain. Another consideration is that many suggested formation mechanisms lead to gas concentration in the very centre of the S0 galaxy during its transformation phase. This has recently been supported by observations suggesting a central starburst (i.e. bulge growth) occurred in many S0s during the process of star formation being quenched in the outer disc (e.g. Bedregal et al. 2011; Johnston et al. 2012, 2014). This process would also lead to an increase in the B/D as the bulge becomes more luminous.

The comparison of our B–D decompositions for Type III S0s with those for the Type III spiral galaxies from Maltby et al. (2012b) should build on these ideas and provide some further insight into the potential processes by which spiral galaxies transform into S0s. In the following, we highlight two key observations from our results:

(i) *S0s generally have a higher B/D than spiral galaxies:* our B–D decompositions indicate that the fraction of bulge-dominated $\mu(r)$ profiles is larger in S0s than spiral galaxies, and that spiral galaxies have mainly disc-dominated $\mu(r)$ profiles. This observation is in agreement with various similar observations by previous works (e.g. Simien & de Vaucouleurs 1986; Laurikainen et al. 2010). With respect to S0 formation theories, this result is consistent with both a fading stellar disc and a central starburst (i.e. bulge growth). Consequently, it appears a galaxy undergoing a spiral → S0 transformation should naturally evolve into a more bulge-dominated system.

(ii) *Bulge light can account for more Type III profiles in S0s than spiral galaxies:* our results suggest that an extended bulge component can account for Type III features in as many as ∼ 45 per cent of Type III S0s, but in only ∼ 15 per cent of Type III spirals (Maltby et al. 2012b). This result can also be understood by the concept of a fading stellar disc as spirals transform into S0s. As the stellar disc fades, the B/D increases and consequently the tail end of the bulge profile may eventually dominate over the disc at large radii (i.e. as in Type C/D profiles; see Fig. 13). This process would naturally lead to an increase in the fraction of Type III-s profiles in S0 galaxies. Currently, it is uncertain as to whether the disc could fade to the required degree in order for this to occur. However, this result is difficult to understand using only the concept of a central starburst (i.e. bulge growth) since the outer regions of the bulge should not be affected in this scenario. Consequently, it appears some disc fading may be required to in order to explain this result.

We note that the fading stellar disc hypothesis is also consistent with the other structural comparisons presented in Section 6 for spiral and S0 galaxies. A fading stellar disc would preserve the disc scalelength. Therefore, the scalelength of Type I profiles would be expected to be independent of morphology (see Fig. 9). For Type II profiles, the suppression of star formation would cause a fading (ageing) of the 'break region' with respect to the inner/outer discs, leading to a convergence of M/L across the $\mu(r)$ break. This would cause the Type II feature to get weaker and may even disappear. Consequently, the observation that Type II profiles are weaker/rarer in S0s compared to spiral galaxies is also consistent with this scenario (see Section 6.2 and Fig. 11). We therefore conclude that in addition a central starbust (i.e. bulge growth), a fading stellar disc seems to

be an inherent process in the morphological transformation of spiral galaxies into S0s.

8 CONCLUSIONS

We present an analysis of V-band radial surface brightness profiles $\mu(r)$ for S0 galaxies from the field and cluster environment using *HST*/ACS imaging and data from the STAGES survey. Using a large, mass-limited ($M_* > 10^9$ M$_\odot$), visually classified sample of ~ 280 field and cluster S0s, we assess the effect of the galaxy environment on the shape of S0 $\mu(r)$ profiles and the structure of S0 stellar discs. We also compare the structure of our S0 stellar discs with those for spiral galaxies from our previous works in order to provide insight into the potential evolutionary mechanisms by which spiral galaxies evolve into S0s.

8.1 Environmental analyses: S0 galaxies

We classify our S0s according to μ break features in their $\mu(r)$ profiles and find that the frequency of profile types (Type I, II and III) is approximately the same in both the field and cluster environments. For both field and cluster S0s, ~ 25 per cent have a simple exponential profile (Type I), < 5 per cent exhibit a down-bending break (truncation, Type II) and ~ 50 per cent exhibit an up-bending break (antitruncation, Type III). For the remaining S0 galaxies (~ 20 per cent), no discernible exponential component was observed (i.e. general curvature in the μ profile, Type c). These profile fractions are robust to the subjective nature of the profile classifications, agreeing for classifications performed by three independent assessors. We also find that limiting our analysis to only low-axis ratio systems ($q > 0.5$) has no significant effect on our profile fractions. These results imply that the shape of S0 $\mu(r)$ profiles is not dependent on the galaxy environment.

The distinct lack of truncations (Type II profiles) in both our field and cluster S0s is of particular interest. In previous works on the disc structure of *spiral* galaxies (e.g. Pohlen & Trujillo 2006; Erwin et al. 2008; Gutiérrez et al. 2011), Type II profiles are very common with the distribution of profile types I:II:III being approximately 20:50:30$\pm$10 per cent. Therefore, it seems whatever mechanism transforms spiral galaxies into S0s may erase these truncations from their $\mu(r)$ profiles. We shall return to this result in Section 8.2. This result is in partial agreement with a similar result reported recently by Erwin et al. (2012), who find no Type II S0s in the cluster environment but a Type II S0 fraction of ~ 30 per cent in the field. Therefore, our Type II S0 fractions are in perfect agreement with Erwin et al. (2012) for the cluster environment, but differ significantly for the field. The origin of this disagreement is uncertain but may be related to the lower fraction of barred S0s (and hence bar-related truncations) in our field sample.

For S0s with a pure exponential disc (Type I), we find no evidence to indicate that the disc scalelength h is dependent on the galaxy environment. Additionally, for S0s with an antitruncated disc (Type III) we find no evidence to suggest any environmental dependence on either the break surface brightness $\mu_{\rm brk}$ or the break strength T (outer-to-inner scalelength ratio, $\log_{10} h_{\rm out}/h_{\rm in}$). These results have been shown to be robust to the error in the sky subtraction and the subjective nature of the profile classifications. We also find that limiting our analysis to only low-axis-ratio systems ($q > 0.5$) has no effect on these results. Therefore, we conclude that there is no evidence to suggest that the stellar distribution in the stellar disc of S0 galaxies is directly affected by the galaxy environment.

These results are consistent with our analogous work, Maltby et al. (2012a), which reaches the same conclusion but for a sample of *spiral* galaxies from STAGES. Our results are also consistent with other studies carried out on the effect of the galaxy environment on disc features in the STAGES survey. For example, Marinova et al. (2009) find that the optical fraction of bars among disc galaxies show no evidence for any strong variation between the field and the A901/2 clusters, suggesting the mass redistribution associated with bar formation within galactic discs is not a strong function of environment from the general field to the intermediate densities of the A901/2 clusters.

However, our results are for one survey field (STAGES), and one multicluster complex of intermediate galaxy density at low redshift ($z \sim 0.167$). Therefore, it is important to investigate whether we see the same trends observed in the STAGES A901/2 field in other survey fields across a wide range of redshift and cluster mass. Extending these studies to higher redshifts is of key importance. In the relatively local Universe, structural evolution in a galaxy's stellar distribution may already have ceased in both the field and cluster environments, even if the environment is the principal driver. However, in the more distant Universe structural changes may still be occurring in both the field and cluster environments and at different rates. Probing denser, more massive cluster environments (e.g. the Coma cluster) is also important because some environmental drivers may only be significant in very high-density environments (i.e. rich cluster cores). Ultimately, the comparison of high-redshift studies with those from the local Universe across a wide range of environments will allow for a complete assessment of whether or not the galaxy environment has any direct effect on a galaxy's stellar distribution.

8.2 Structural analyses: implications for S0 formation

We complement our environmental studies by comparing the structural analyses of our S0s with those for spiral galaxies from our previous works. These comparisons provide some insight into the potential evolutionary paths by which spiral galaxies transform into S0s. Two structural comparisons were made:

(i) *The structure of galactic discs.* We compare the disc structure of our S0s with the spiral galaxies from our analogous work, Maltby et al. (2012a). For spiral/S0 galaxies with a pure exponential disc (Type I), we find no evidence to suggest that the disc scalelength h is dependent on the galaxy morphology. For spiral/S0 galaxies with an antitruncated disc (Type III), we also find no evidence to suggest that the break surface brightness $\mu_{\rm brk}$ is related to the galaxy morphology. However, we do find some evidence (significance $> 3\sigma$) that the break strength T of spiral/S0 galaxies is somehow related to the galaxy morphology, with T for both

Type II and III profiles being generally smaller (weaker) in S0s compared to spiral galaxies.

In order to understand this result, we need to consider the current theory for the formation of stellar disc truncations. For classical truncations (Type II-CT), current theories suggest that their formation is via a radial star-formation threshold and the outward scattering of inner disc stars to regions beyond this threshold (i.e. break radius; Debattista et al. 2006; Bakos et al. 2008; Martínez-Serrano et al. 2009). Consequently, the outer disc should be populated by old stars as these are the ones that have had enough time to make the disc migration. In this scenario, the truncation (Type II feature) is related to a radial change in the age of the stellar population throughout the disc. Assuming this formation scenario, and an inside-out growth for the inner disc [i.e. negative age(r) gradient], the suppression of star formation in the galaxy (e.g. via gas stripping) would cause the age of the stellar population in the 'break region' to increase and the M/L across the $\mu(r)$ break to converge. Consequently, the μ break will get weaker and may even disappear. For bar-related truncations (Type II-OLR), the μ break is expected to be related to a resonance phenomenon and therefore the above scenario does not hold. However, Erwin et al. (2012) suggest that the depletion/removal of gas from a barred galaxy would cause a weakening of the resonance effect and may weaken or remove the Type II-OLR break from the $\mu(r)$ profile. Considering these theories, the absence/weakening of Type II profiles in our S0s may actually be the natural consequence of the termination of star formation in the stellar disc as spiral galaxies transform into S0s. For Type III profiles, the observed weakening may be the consequence of radial mixing throughout the disc related to the suspected minor-merger history of the Type III system.

In order to fully test these hypotheses, we require high-quality colour profiles, or better still stellar age profiles, on a large sample of spiral/S0 galaxies covering a wide range of stellar masses. Only then will we be able to test whether the weakening of the $\mu(r)$ break in S0 galaxies is related to a weakening of their age profile gradient.

(ii) *The nature of antitruncated stellar light profiles.* We also explore the nature of antitruncated (Type III) stellar light profiles in S0 galaxies and assess the effect of a 'classical', de Vaucouleurs (1948) bulge on the outer regions of their $\mu(r)$ profiles. In Type III $\mu(r)$ profiles (up-bending breaks), the excess light beyond the break radius $r_{\rm brk}$ can either be related to an outer exponential disc (Type III-d) or an extended spheroidal component (Type III-s). Using analytical B–D decomposition (de Vaucouleurs, $r^{1/4}$ bulge plus single exponential disc) on a sample of 39 Type III S0s, we assess the *maximum* fraction of Type III S0s for which the excess light at large radii ($r > r_{\rm brk}$) could be caused or affected by the spheroidal component.

Our results indicate that for only about a half of Type III S0s, the antitruncation is related to an outer shallow disc (Type III-d). For the remaining cases, the excess light at $r > r_{\rm brk}$ can be accounted for by the bulge profile (Type III-s). More importantly, for these latter cases there are many S0s ($\sim$ 20 per cent of the Type III subsample) that exhibit an antitruncated $\mu(r)$ profile caused by the bulge profile extending beyond a dominant disc. However, with respect to these results, it is important to note that our adopted methodology (the use of a de Vaucouleurs bulge in our B-D decomposition) leads to an over-estimation of the bulge light in the outer regions of the $\mu(r)$ profile. This naturally enhances the fraction of Type III-s profiles, which therefore represents an upper limit to the fraction of genuine Type III-s profiles in our Type III S0s. Therefore, we conclude that bulge light is an important component in the $\mu(r)$ profiles of many S0s at large radii and that antitruncations in S0 galaxies are commonly caused by either the bulge or disc component. This result is in sharp contrast to the result of Maltby et al. (2012b) for *spiral galaxies* where in the vast majority of cases ($\sim$ 85 per cent), Type III profiles are a true disc phenomenon (i.e. Type III-d).

We propose that these results are consistent with the hypothesis that spiral galaxies transform into S0s by the termination of star formation. The suppression of star formation in the stellar disc (e.g. by gas stripping), would cause the disc component to gradually fade and the B/D to increase. Consequently, any galaxy undergoing a spiral $\rightarrow$ S0 transformation should naturally evolve into a more bulge-dominated system. As the stellar disc fades the tail end of the bulge profile may eventually dominate over the stellar disc at large radii. Consequently, if a fading stellar disc is inherent to the morphological transformation of spirals into S0s, this would naturally lead to an increase in the fraction of antitruncations caused by the bulge component (Type III-s) in S0 galaxies. Alternative processes inherent to the morphological transformation of spirals into S0s, such as a central starburst (Bedregal et al. 2011; Johnston et al. 2012, 2014), could also influence the bulge profile. However, the emergence of the bulge profile over the disc in the *outer* regions implies some degree of disc fading is required. Unfortunately, at present it is uncertain as to whether the disc could fade to the required degree in order for this to occur and stellar population synthesis modelling would be required to study this further.

Taken together, the results of our environmental studies suggest that the galaxy environment has little direct effect on the structure of a galaxy's stellar distribution (at least from the general field to the intermediate densities probed by the STAGES survey). Consequently, our results imply that environmental processes directly affecting the structure of the stellar distribution, i.e. galaxy-galaxy or galaxy-cluster gravitational interactions (e.g. mergers and harassment), are not driving the observed morphology–density relation. The results of our morphological comparisons are also consistent with this finding, implying that a fading stellar disc is a likely process inherent to spiral $\rightarrow$ S0 transformations. This result is also supported by the environmental comparisons of Bösch et al. (2013b), using rotational gas kinematics. Bösch et al. (2013b) find that in the cluster environment, disc galaxies with smooth morphology (i.e. S0s) exhibit greater kinematic disturbances in the gas disc than disc galaxies with greater morphological asymmetry (i.e. spirals). This suggests that a subtle cluster-related gas process (e.g. ram-pressure stripping) is directly affecting the gaseous disc of cluster galaxies. Such processes could cause star formation to be quenched in the stellar disc and bring about disc fading. Consequently, we conclude that more subtle processes acting on the gaseous component of a galaxy (e.g.

ram-pressure stripping) are more likely to play an important role in the origin of the morphology–density relation and the transformation of spiral galaxies into S0s.

9 ACKNOWLEDGEMENTS

We thank the anonymous referee for their detailed and insightful comments on the original version of this manuscript, which helped to improve it considerably. The support for STAGES was provided by NASA through GO-10395 from STScI operated by AURA under NAS5-26555. DTM was supported by STFC. MEG was supported by an STFC Advanced Fellowship. AB acknowledges the funding of the Austrian Science Foundation FWF (projects P19300-N16 and P23946-N16).

REFERENCES

Allen P. D., Driver S. P., Graham A. W., Cameron E., Liske J., de Propris R., 2006, MNRAS, 371, 2
Aragón-Salamanca A., Bedregal A. G., Merrifield M. R., 2006, A&A, 458, 101
Azzollini R., Trujillo I., Beckman J. E., 2008, ApJ, 684, 1026
Bakos J., Trujillo I., Pohlen M., 2008, ApJ, 683, L103
Barden M., Häußler B., Peng C. Y., McIntosh D. H., Guo Y., 2012, MNRAS, 422, 449
Bedregal A. G., Cardiel N., Aragón-Salamanca A., Merrifield M. R., 2011, MNRAS, 415, 2063
Bertola F., Vietri M., Zeilinger W. W., 1991, ApJ, 374, L13
Bland-Hawthorn J., Vlajić M., Freeman K. C., Draine B. T., 2005, ApJ, 629, 239
Borch A., et al., 2006, A&A, 453, 869
Bösch B., et al., 2013a, A&A, 549, A142
Bösch B., et al., 2013b, A&A, 554, A97
Bournaud F., Elmegreen B. G., Elmegreen D. M., 2007, ApJ, 670, 237
Brown L. D., Cai T. T., DasGupta A., 2001, Stat. Sci., 16, 101
Buitrago F., Trujillo I., Conselice C. J., Bouwens R. J., Dickinson M., Yan H., 2008, ApJ, 687, L61
de Vaucouleurs G., 1948, Annales d'Astrophysique, 11, 247
de Vaucouleurs G., 1959, Handbuch der Physik, 53, 311
Debattista V. P., Mayer L., Carollo C. M., Moore B., Wadsley J., Quinn T., 2006, ApJ, 645, 209
Dressler A., 1980, ApJ, 236, 351
Elmegreen B. G., Parravano A., 1994, ApJ, 435, L121
Erwin P., Beckman J. E., Pohlen M., 2005, ApJ, 626, L81
Erwin P., Gutiérrez L., Beckman J. E., 2012, ApJ, 744, L11
Erwin P., Pohlen M., Beckman J. E., 2008, AJ, 135, 20
Faber S. M., 1973, ApJ, 179, 423
Ferguson A., Irwin M., Chapman S., Ibata R., Lewis G., Tanvir N., 2007, in de Jong, R. S., ed., Island Universes: Structure and Evolution of Disk Galaxies. Springer, Dordrecht, p. 239
Freeman K. C., 1970, ApJ, 160, 811
Gray M. E., et al., 2009, MNRAS, 393, 1275
Gunn J. E., Gott J. R. I., 1972, ApJ, 176, 1
Gutiérrez L., Erwin P., Aladro R., Beckman J. E., 2011, AJ, 142, 145
Heiderman A., et al., 2009, ApJ, 705, 1433
Hoyos C., et al., 2012, MNRAS, 419, 2703
Ibata R., Chapman S., Ferguson A. M. N., Lewis G., Irwin M., Tanvir N., 2005, ApJ, 634, 287
Icke V., 1985, A&A, 144, 115
Johnston E. J., Aragón-Salamanca A., Merrifield M. R., 2014, MNRAS, 441, 333
Johnston E. J., Aragón-Salamanca A., Merrifield M. R., Bedregal A. G., 2012, MNRAS, 422, 2590
Kennicutt Jr. R. C., 1989, ApJ, 344, 685
Kron R. G., 1980, ApJS, 43, 305
Larson R. B., Tinsley B. M., Caldwell C. N., 1980, ApJ, 237, 692
Laurikainen E., Salo H., Buta R., Knapen J. H., Comerón S., 2010, MNRAS, 405, 1089
Maltby D. T., et al., 2010, MNRAS, 402, 282
Maltby D. T., et al., 2012a, MNRAS, 419, 669
Maltby D. T., Hoyos C., Gray M. E., Aragón-Salamanca A., Wolf C., 2012b, MNRAS, 420, 2475
Marinova I., et al., 2009, ApJ, 698, 1639
Martínez-Serrano F. J., Serna A., Doménech-Moral M., Domínguez-Tenreiro R., 2009, ApJ, 705, L133
Mihos J. C., Hernquist L., 1994, ApJ, 425, L13
Moore B., Katz N., Lake G., Dressler A., Oemler A., 1996, Nature, 379, 613
Peng C. Y., Ho L. C., Impey C. D., Rix H.-W., 2002, AJ, 124, 266
Pérez I., 2004, A&A, 427, L17
Pohlen M., Dettmar R., Lütticke R., Aronica G., 2002, A&A, 392, 807
Pohlen M., Trujillo I., 2006, A&A, 454, 759
Pohlen M., Zaroubi S., Peletier R. F., Dettmar R., 2007, MNRAS, 378, 594
Roškar R., Debattista V. P., Quinn T. R., Stinson G. S., Wadsley J., 2008b, ApJ, 684, L79
Roškar R., Debattista V. P., Stinson G. S., Quinn T. R., Kaufmann T., Wadsley J., 2008a, ApJ, 675, L65
Schaye J., 2004, ApJ, 609, 667
Sérsic J. L., 1968, Atlas de galaxias australes. Cordoba, Argentina: Observatorio Astronomico, 1968
Sil'Chenko O. K., Chilingarian I. V., Sotnikova N. Y., Afanasiev V. L., 2011, MNRAS, 414, 3645
Simien F., de Vaucouleurs G., 1986, ApJ, 302, 564
Trujillo I., Pohlen M., 2005, ApJ, 630, L17
van der Kruit P. C., 1979, A&AS, 38, 15
Weinmann S. M., van den Bosch F. C., Yang X., Mo H. J., 2006, MNRAS, 366, 2
Wilson E. B., 1927, J. Am. Stat. Assoc., 22, 209
Wolf C., et al., 2004, A&A, 421, 913
Wolf C., et al., 2009, MNRAS, 393, 1302
Wolf C., Hildebrandt H., Taylor E. N., Meisenheimer K., 2008, A&A, 492, 933
Wolf C., Meisenheimer K., Rix H.-W., Borch A., Dye S., Kleinheinrich M., 2003, A&A, 401, 73
Younger J. D., Cox T. J., Seth A. C., Hernquist L., 2007, ApJ, 670, 269

This paper has been typeset from a TEX/ LATEX file prepared by the author.